Evaluation of bacterial glycerol dialkyl glycerol tetraether and ^{2}H-^{18}O biomarker proxies along a Central European topsoil transect

Johannes Hepp[1,2,*], Imke K. Schäfer[3], Verena Lanny[4], Jörg Franke[3], Marcel Bliedtner[3,a], Kazimierz Rozanski[5], Bruno Glaser[2], Michael Zech[2,6], Timothy I. Eglinton[4], Roland Zech[3,a]

[1]Chair of Geomorphology and BayCEER, University of Bayreuth, 95440 Bayreuth, Germany and
[2]Institute of Agronomy and Nutritional Sciences, Soil Biogeochemistry, Martin-Luther-University Halle-Wittenberg, 06120 Halle, Germany
[3]Institute of Geography and Oeschger Centre for Climate Change Research, University of Bern, 3012 Bern, Switzerland
[4]Department of Earth Science, ETH Zurich, 8092 Zurich, Switzerland
[5]Faculty of Physics and Applied Computer Science, AGH University of Science and Technology, 30-059 Kraków, Poland
[6]Institute of Geography, Faculty of Environmental Sciences, Technical University of Dresden, 01062 Dresden, Germany
[a]now at Institute of Geography, Chair of Physical Geography, Friedrich-Schiller University of Jena, 07743 Jena, Germany

*corresponding author (johannes-hepp@gmx.de)

Keywords

Leaf wax *n*-alkanes, hemicellulose sugars, pH, temperature, CBT, MBT', precipitation δ^2H and $\delta^{18}O$, relative humidity

Abstract

Molecular fossils, like bacterial branched glycerol dialkyl glycerol tetraethers (brGDGTs), and the stable isotopic composition of biomarkers, such as δ^2H of leaf wax-derived *n*-alkanes ($\delta^2H_{n\text{-alkane}}$) or $\delta^{18}O$ of hemicellulose-derived sugars ($\delta^{18}O_{sugar}$) are increasingly used for the reconstruction of past climate and environmental conditions. Plant-derived $\delta^2H_{n\text{-alkane}}$ and $\delta^{18}O_{sugar}$ values record the isotopic composition of plant source water ($\delta^2H_{source\text{-}water}$ and $\delta^{18}O_{source\text{-}water}$), which usually reflects mean annual precipitation ($\delta^2H_{precipiation}$ and $\delta^{18}O_{precipiation}$), modulated by evapotranspirative leaf water enrichment and biosynthetic fractionation. Accuracy and precision of respective proxies should be ideally evaluated at a regional scale. For this study, we analysed topsoils below coniferous and deciduous forests, as well as grassland soils along a Central European transect in order to investigate the variability and robustness of various proxies, and to identify effects related to vegetation. Soil pH-values derived from brGDGTs correlate reasonably well with measured soil pH-values, but systematically overestimate them (ΔpH = 0.6 ±0.6). The branched vs. isoprenoid tetraether index (BIT) can give some indication whether the pH reconstruction is reliable. Temperatures derived from brGDGTs overestimate mean annual air temperatures slightly (ΔT_{MA} = 0.5°C ±2.4). Apparent isotopic fractionation ($\varepsilon_{n\text{-alkane/precipitation}}$ and $\varepsilon_{sugar/precipitation}$) is lower for grassland sites than for forest sites due to "signal damping", i.e. grass biomarkers do not record the full evapotranspirative leaf water enrichment. Coupling $\delta^2H_{n\text{-alkane}}$ with $\delta^{18}O_{sugar}$ allows to reconstruct the stable isotopic composition of the source water more accurately than without the coupled approach ($\Delta\delta^2H$ = ~-21‰ ±22 and $\Delta\delta^{18}O$ = ~-2.9‰ ±2.8). Similarly, relative humidity during daytime and vegetation period (RH_{MDV}) can be reconstructed using the coupled isotope approach (ΔRH_{MDV} = ~-17 ±12). Especially for coniferous sites, reconstructed RH_{MDV} values as well as source water isotope composition underestimate the measured values. This can be likely explained by understory grass vegetation at the coniferous sites contributing significantly to the *n*-alkane pool but only marginally to the sugar pool in the topsoils. Furthermore, vegetation-dependent variable "signal damping" and ε_{bio} along our European transect are difficult to quantify quantitatively but likely do contribute like microclimate variability to the rather large uncertainties in the source water isotope composition and RH reconstructions. Vegetation-related effects do, by contrast, likely not affect the brGDGT-derived reconstructions. Overall, GDGTs and the coupled $\delta^2H_{n\text{-alkane}}$-$\delta^{18}O_{sugar}$ approach have great potential for more quantitative paleoclimate reconstructions.

1 Introduction

Information about the variability and consequences of past climate changes is a prerequisite for precise predictions regarding the present climate change. Molecular fossils, so called biomarkers, have great potential to enhance our understanding about variations of past climate and environmental changes. Lipid biomarkers in particular are increasingly used for paleoclimate and environmental reconstructions (e.g. Brincat et al., 2000; Eglinton and Eglinton, 2008; Rach et al., 2014; Romero-Viana et al., 2012; Schreuder et al., 2016). However strengths and limitations of respective proxies need to be known (Dang et al., 2016). For this, calibrations using modern reference samples are essential.

One famous and widely applied lipid biomarker group are terrestrial branched glycerol dialkyl glycerol tetraethers (brGDGTs). They are synthesized in the cell membranes of anaerobe heterotrophic soil bacteria (Oppermann et al., 2010; Weijers et al., 2010) have great potential for the reconstruction of past environmental conditions (e.g. Coffinet et al., 2017; Schreuder et al., 2016; Zech et al., 2012), although some uncertainties exist. Calibration studies suggest that the relative abundance of the individual brGDGTs varies with mean annual air temperature (T_{MA}) and soil pH (Peterse et al., 2012; Weijers et al., 2007), at least across large, global climate gradients or along pronounced altitudinal gradients (Wang et al., 2017). However, in arid regions the production of brGDGT is limited, while isoprenoidal GDGTs (iGDGTs) produced by archaea provide the dominant part of the overall soil GDGT pool (Anderson et al., 2014; Dang et al., 2016; Dirghangi et al., 2013; Wang et al., 2013; Xie et al., 2012). The ratio of brGDGTs vs. isoprenoid GDGTs (BIT) can be used as indication whether a reconstruction of T_{MA} and pH will be reliable. Moreover, Mueller-Niggemann et al. (2016) revealed an influence of the vegetation cover on the brGDGT producing soil microbes. From field experiments, it is known that vegetation type and mulching practice strongly effect soil temperature and moisture (Awe et al., 2015; Liu et al., 2014). Thus, multiple factors can be expected to influence soil microbial communities and GDGT production. So far, little is known about the variability of GDGT proxies on a regional scale, and a calibration study with small climate gradient but with different vegetation types might be useful.

Concerning paleohydrology proxies, compound specific stable hydrogen isotopes of leaf wax biomarkers, such as long chain *n*-alkanes ($\delta^2H_{n\text{-alkanes}}$) record the isotopic signal of precipitation and therefore past climate and environmental conditions (Sachse et al., 2004, 2006). However, various influencing factors are known e.g. the moisture source to leaf waxes (Pedentchouk and Zhou, 2018 and Sachse et al., 2012 for review). Next is the evapotranspiration of leaf water (Feakins and Sessions, 2010; Kahmen et al., 2013; Zech et al., 2015), which is strongly driven by relative air humidity (RH; e.g. Cernusak et al., 2016 for review). In addition, a strong precipitation signal is known to be incorporated into long chain leaf waxes (Hou et al., 2008; Rao et al., 2009; Sachse et al., 2004). In paleoclimate studies, it is often not feasible to disentangle between the evapotranspirative enrichment from the precipitation signal. Zech et al. (2013) proposed to couple $\delta^2H_{n\text{-alkane}}$ results with oxygen stable isotopes of hemicellulose-derived sugars ($\delta^{18}O_{sugar}$). Assuming constant biosynthetic fractionation factors (ε_{bio}) for the different compound classes (*n*-alkanes and hemicellulose sugars), the coupling enables the reconstruction of the isotopic composition of leaf water, RH and δ^2H and $\delta^{18}O$ of plant source water ($\approx \delta^2H$ and $\delta^{18}O$ of precipitation; Tuthorn et al., 2015). So far, a detailed evaluation of

this approach on the European scale, as well as related effects concerning vegetation changes is missing.

We analysed topsoil samples under coniferous, deciduous and grassland vegetation along a Central European transect in order to estimate the variability of the biomarker proxies. More specifically, we aim to test whether:

(i) the vegetation type has an influence on the brGDGT proxies, the $\delta^2H_{n\text{-alkane}}$ and the $\delta^{18}O_{sugar}$ stable isotopic composition, as well as on reconstructed $\delta^2H_{source\text{-}water}$, $\delta^{18}O_{source\text{-}water}$ and RH.

(ii) the published brGDGT proxies used for reconstructing mean annual temperature and soil pH are sensitive enough to reflect the medium changes in temperature and soil pH along our transect.

(iii) the coupled $\delta^2H_{n\text{-alkane}}$-$\delta^{18}O_{sugar}$ approach enables a δ^2H and $\delta^{18}O$ of precipitation and RH reconstruction along the transect.

2 Material and methods

2.1 Geographical setting and sampling

In November 2012, we collected 29 topsoil samples (0-5 cm depth) from 16 locations along a transect from Southern Germany to Southern Sweden (Fig. 1A). We distinguished between sites with coniferous forest (con, n = 9), deciduous forest (dec, n = 14) and grassland (grass, n = 6) vegetation cover (for more details see Schäfer et al. (2016) and Tab. S1).

2.2 Database of instrumental climate variables and isotope composition of precipitation

Climate data was derived from close-by weather observation stations operating by the regional institutions (Deutscher Wetterdienst (DWD) for Germany, Danmarks Meteorologiske Institut (DMI) for Denmark and the Sveriges Meteorologiska och Hydrologiska Institute (SMHI) for Sweden). The DWD provides hourly data for each station (DWD Climate Data Center, 2018b), enabling not only the calculation of T_{MA}, but also of the mean annual relative air humidity (RH_{MA}), mean temperature and relative air humidity during the vegetation period (T and RH_{MV}), and of daytime temperature and relative humidity averages over the vegetation period (T and RH_{MDV}). In addition, annual precipitation observations were used to derive the mean annual precipitation amount (P_{MA}; DWD Climate Data Center, 2018b). From the DMI, the respective climate variables were derived from published technical reports (Cappelen, 2002; Frich et al., 1997; Laursen et al., 1999). The SMHI provides open data from which we derived the climate variables for the Swedish sites (Swedish Meteorological and Hydrological Institute, 2018). For more details about the climate database used for calculations and comparisons, the reader is referred to Tab. S2.

For comprising German precipitation $\delta^2H/\delta^{18}O$ along the transect, we realized a regionalisation (called δ^2H_{GIPR} and $\delta^{18}O_{GIPR}$) using online available data from 34 German GNIP stations, 4 Austrian ANIP stations and the Groningen GNIP station (van Geldern et al., 2014; IAEA/WMO, 2018; Stumpp et al., 2014; Umweltbundesamt GmbH, 2018), following the approach of Schlotter (2007). However, instead of the multivariate regression procedure applied

by Schlotter (2007), we used a random forest approach (Hothorn et al., 2006; Strobl et al., 2007, 2008) to describe the relationship of squared latitude, latitude, longitude and altitude vs. long term weighted means of precipitation δ^2H and $\delta^{18}O$, and realized the prediction for each site (see supplementary method description for more information). For the Danish and Swedish sites, such a procedure was not possible. Hence, the annual precipitation δ^2H and $\delta^{18}O$ values were derived from the Online Isotopes in Precipitation Calculator (OIPC, version 3.1), therefore called δ^2H_{OIPC} and $\delta^{18}O_{OIPC}$ (Bowen, 2018; Bowen and Revenaugh, 2003; IAEA/WMO, 2015). The finally used $\delta^2H_{GIPR,OIPC}$ and $\delta^{18}O_{GIPR,OIPC}$ data are given in Tab. S1.

The T_{MA} along the transect ranges from 5.3 to 10.6°C, and P_{MA} ranges from 554 to 1769 mm (Fig. 1B). Precipitation $\delta^2H/\delta^{18}O$ shows moderate changes along the transect, $\delta^2H_{GIPR/OIPC}$ varies between -52 and -79‰, and $\delta^{18}O_{GIPR/OIPC}$ ranges from -7.4 to -10.9‰ (Fig. 1C).

Correlations between $\delta^{18}O_{GIPR/OIPC}$ and P_{MA}, altitude of the locations, T_{MA} are given in the supplementary material (Fig. S1 to S3), along with a $\delta^2H_{GIPR/OIPC}$ vs. $\delta^{18}O_{GIPR/OIPC}$ scatter plot (Fig. S4).

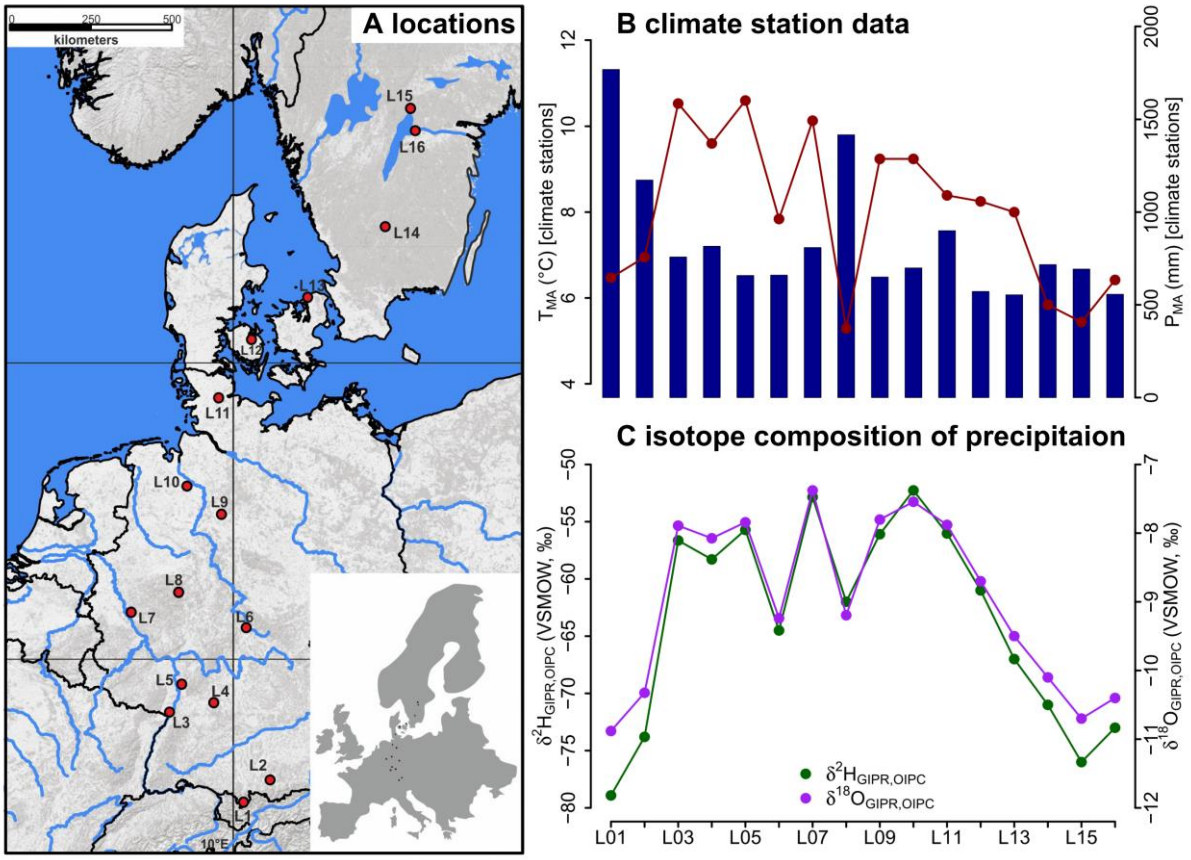

Fig. 1. (A) Sample locations (red dots, map source: US National Park Service), (B) variations of mean annual air temperature (T_{MA}, red dots and line) and mean annual precipitation (P_{MA}, blue bars) derived from close-by climate station data, and (C) hydrogen and oxygen stable isotope composition of precipitation ($\delta^2H_{GIPR/OIPC}$ and $\delta^{18}O_{GIPR/OIPC}$, respectively) as derived for the sampled transect locations (see section 2.2 GIPR δ^2H and $\delta^{18}O$ generation procedure). The reader is referred to section 2.2 (and Tab. S1 and S2) for database and reference information of data plotted in (B) and (C).

2.3 Soil extractions and analysis

2.3.1 GDGTs and pH

A detailed description of sample preparation for lipid analysis can be found in Schäfer et al. (2016). Briefly, 1–6 g freeze-dried and grounded soil sample was microwave extracted with 15 ml dichloromethane (DCM)/methanol (MeOH) 9:1 *(v:v)* at 100°C for 1 h. Extracts were separated over aminopropyl silica gel (Supelco, 45 μm) pipette columns. The nonpolar fraction (including *n*-alkanes) was eluted with hexane and further purified over $AgNO_3$ coated silica pipette columns (Supelco, 60-200 mesh) and zeolite (Geokleen Ltd.). The GDGT-containing fraction was eluted with DCM:MeOH 1:1 *(v:v)*, re-dissolved in hexane/isopropanol (IPA) 99:1 *(v:v)* and transferred over 0.45 μm PTFE filters into 300 μl inserts. For quantification, a known amount of a C_{46} diol standard was added after transfer. The samples were analysed at ETH Zurich using an Agilent 1260 Infinity series HPLC–atmospheric chemical pressure ionization mass spectrometer (HPLC–APCI-MS) equipped with a Grace Prevail Cyano column (150 mm × 2.1 mm; 3 μm). The GDGTs were eluted isocratically with 90% A and 10% B for 5 min and then with a linear gradient to 18% B for 34 min at 0.2 ml min^{-1}, where A=hexane and B=hexane/isopropanol (9:1, *v:v*). Injection volume was 10 μl and single ion monitoring of $[M+H]^+$ was used to detect GDGTs.

The pH of the samples was measured in the laboratory of the Soil Biogeochemistry group, Institute of Agronomy and Nutritional Sciences, Martin-Luther-University Halle-Wittenberg, using a pH meter in a 1:3 soil:water *(w/v)* mixture.

2.3.2 $\delta^2H_{n\text{-alkane}}$

The hydrogen isotopic composition of the highest concentrated *n*-alkanes (*n*-C_{25}, *n*-C_{27}, *n*-C_{29}, *n*-C_{31}, and *n*-C_{33}) was determined using a TRACE GC Ultra Gas Chromatography connected to a Delta V Plus Isotope Ratio Mass Spectrometer via a ^2H pyrolysis reactor kept at 1420 °C (GC-^2H-Py-IRMS; Thermo Scientific, Bremen, Germany) at ETH Zurich (Christoph et al., 2019). For more details about *n*-alkane quantification the reader is refereed to Schäfer et al. (2016). The compound-specific $^2H/^1H$ ratios were calibrated against an external standard with $C_{15} – C_{35}$ homologues. External standard mixtures (A4 mix from A. Schimmelmann, University of Indiana) were run between the samples for multipoint linear normalization. The H^+_3 factor was determined on each measurement day and was constant throughout the periods of the sample batches. Samples were analysed in duplicates, and results typically agreed within 4% (average difference = 1.4%). All δ^2H values are expressed relative to the Vienna Standard Mean Ocean Water (V-SMOW).

2.3.3 $\delta^{18}O_{sugar}$

Hemicellulose sugars were extracted and purified using a slightly modified standard procedure (Amelung et al., 1996; Guggenberger et al., 1994; Zech and Glaser, 2009). Briefly, myoinositol was added to the samples prior to extraction as first internal standard. The sugars were released hydrolytically using 4M trifluoroacetic acid for 4 h at 105°C, cleaned over glass fiber filters and further purified using XAD and Dowex columns. Before derivatization with methylboronic acid (Knapp, 1979), the samples were frozen, freeze-dried, and 3-O-methylglucose in dry pyridine

was added as second internal standard. Compound-specific hemicellulose sugar ^{18}O measurements were performed in the laboratory of the Soil Biogeochemistry group, Institute of Agronomy and Nutritional Sciences, Martin-Luther-University Halle-Wittenberg, using GC-^{18}O-Py-IRMS (all devices from Thermo Fisher Scientific, Bremen, Germany). Standard deviations of the triplicate measurements were 1.4‰ (over 29 investigated samples) for arabinose and xylose, respectively. We focus on these two hemicellulose-derived neutral sugars arabinose and xylose as they strongly predominate over fucose in terrestrial plants, soils and sediments (Hepp et al., 2016 and references therein). Rhamnose concentrations were too low to obtain reliable $\delta^{18}O$ results. All $\delta^{18}O$ values are expressed relative to the Vienna Standard Mean Ocean Water (V-SMOW).

2.4 Theory and Calculations

2.4.1 Calculations used for the GDGT-based reconstructions

The branched and isoprenoid tetraether (BIT) index is calculated according to Hopmans et al. (2004), for structures see Fig. S5:

$$BIT = \frac{Ia+IIa+IIIa}{Ia+IIa+IIIa+crenarchaeol}. \quad (1)$$

The cyclopentane moiety number of brGDGTs correlates negatively with soil pH (Weijers et al., 2007), which led to the development of the cyclization of branched tetraethers (CBT) ratio. CBT and the CBT based pH (pH_{CBT}) were calculated according to Peterse et al. (2012):

$$CBT = -\log\frac{Ib+IIb}{Ia+IIa}, \quad (2)$$

$$pH_{CBT} = 7.9 - 1.97 \times CBT. \quad (3)$$

The number of methyl groups in brGDGTs correlates negatively with T_{MA} and soil pH (Peterse et al., 2012; Weijers et al., 2007). Thus, the ratio of the methylation of branched tetraethers (MBT) ratio and the CBT ratio can be used to reconstruct T_{MA}. We use the equation given by Peterse et al. (2012):

$$MBT' = \frac{Ia+Ib+Ic}{Ia+Ib+Ic+IIa+IIb+IIc+IIIa}, \quad (4)$$

$$T_{MA} = 0.81 - 5.67 \times CBT + 31.0 \times MBT'. \quad (5)$$

2.4.2 Calculations and concepts used for the coupled δ^2H-$\delta^{18}O$ approach

The apparent fractionation is calculated according to Cernusak et al. (2016):

$$\varepsilon_{n\text{-alkane/precipitation}} = \left(\frac{\delta^2H_{n\text{-alkane}} - \delta^2H_{GIPR,OIPC}}{1+\delta^2H_{GIPR,OIPC}/1000}\right), \quad (6)$$

$$\varepsilon_{sugar/precipitation} = \left(\frac{\delta^{18}O_{sugar} - \delta^{18}O_{GIPR,OIPC}}{1+\delta^{18}O_{GIPR,OIPC}/1000}\right). \quad (7)$$

The isotopic composition of leaf water ($\delta^2H_{leaf\text{-}water}$ and $\delta^{18}O_{leaf\text{-}water}$) can be calculated using ε_{bio} for $\delta^2H_{n\text{-alkane}}$ (-160‰, Sachse et al., 2012; Sessions et al., 1999) and $\delta^{18}O_{sugar}$ (+27‰, Cernusak et al., 2003; Schmidt et al., 2001):

$$\delta^2H_{leaf\text{-}water} = \left(\frac{1000+\delta^2H_{n\text{-alkane}}}{1000+\varepsilon_{bio}\ (n\text{-alkane})}\right) \times 10^3 - 1000, \quad (8)$$

$$\delta^{18}O_{leaf\text{-}water} = \left(\frac{1000+\delta^{18}O_{sugar}}{1000+\varepsilon_{bio\ (sugar)}}\right) \times 10^3 - 1000. \quad (9)$$

Zech et al. (2013) introduced the conceptual model for the coupled $\delta^2H_{n\text{-alkane}}$-$\delta^{18}O_{sugar}$ approach in detail. Briefly, the coupled approach is based on the following assumptions (illustrated in Fig. 8): (i) The isotopic composition of precipitation, which is set to be equal to the plant source water, typically plots along the global meteoric water line (GMWL; $\delta^2H = 8 \times \delta^{18}O + 10$) in a $\delta^{18}O$ vs. δ^2H space (Craig, 1961); (ii) Source water uptake by plants does not lead to any fractionation (e.g. Dawson et al., 2002), and significant evaporation of soil water can be excluded; (iii) Evapotranspiration leads to enrichment of the remaining leaf water along the local evaporation line (LEL; Allison et al., 1985; Bariac et al., 1994; Walker and Brunel, 1990), compared to the source water taken up by the plant; (iv) The biosynthetic fractionation is assumed to be constant. In addition, isotopic equilibrium between plant source water (~ weighted mean annual precipitation) and the local atmospheric water vapour is assumed. Further assumption concerns the isotope steady-state in the evaporating leaf water reservoir. The coupled approach allows for reconstructing the isotopic composition of plant source water ($\delta^2H_{source\text{-}water}$ and $\delta^{18}O_{source\text{-}water}$) from the reconstructed leaf water, by calculating the intercepts of the LELs with the GMWL (Zech et al., 2013). The slope of the LEL (S_{LEL}) can be assessed by the following equation (Gat, 1971):

$$S_{LEL} = \frac{\varepsilon_2^* + C_k^2}{\varepsilon_{18}^* + C_k^{18}}, \quad (10)$$

where ε* are equilibrium isotope fractionation factors and C_k are kinetic fractionation factors. The latter equals to 25.1‰ and 28.5‰, for C_k^2 and C_k^{18}, respectively (Merlivat, 1978). The equilibrium fractionation factors can be derived from empirical equations (Horita and Wesolowski, 1994) by using T_{MDV} values. For two Danish sites T_{MDV} are not available, instead T_{MV} is used here (section 2.2 and Tab. S2).

In a $\delta^{18}O$-δ^2H diagram, the distance of the leaf water from the GMWL define the deuterium-excess of leaf water ($d_{leaf\text{-}water} = \delta^2H_{leaf\text{-}water} - 8 \times \delta^{18}O_{leaf\text{-}water}$, according Dansgaard, (1964); Fig. 8). To convert $d_{leaf\text{-}water}$ into mean RH during daytime and vegetation period (RH_{MDV}), a simplified Craig-Gordon model can be applied (Zech et al., 2013):

$$RH = 1 - \frac{\Delta d}{\varepsilon_2^* - 8 \times \varepsilon_{18}^* + C_k^2 - 8 \times C_k^{18}}, \quad (11)$$

where Δd is the difference in $d_{leaf\text{-}water}$ and the deuterium-excess of source water ($d_{source\text{-}water}$).

2.5 Statistics

In the statistical analysis we checked sample distributions for normality (Shapiro and Wilk, 1965) and for equal variance (Levene, 1960). If normality and equal variances are given, we perform an Analysis of Variance (ANOVA). If that is not the case, we conduct the non-parametric Kruskal-Wallis Test. ANOVA or Kruskal-Wallis are used to find significant differences (a=0.05) between the vegetation types (deciduous, conifer and grass).

In order to describe the relation along a 1:1 line, the coefficient of correlation (R^2) was calculated as $R^2 = 1 - \sum(\text{modeled} - \text{measured})^2 / \sum(\text{measured} - \text{measured mean})^2$. The small r^2 is taken as coefficient of correlation of a linear regression between a dependent (y) and

explanatory variable(s). The root mean square error (RMSE) of the relationships was calculated as $\mathrm{RMSE} = \sqrt{\left(\frac{1}{n} \cdot \sum(\text{modeled - measured})^2\right)}$. All data plotting and statistical analysis was realized in R (version 3.2.2; R Core Team, 2015).

3 Results and Discussion

3.1 GDGT concentrations

GDGT Ia has the highest concentration under all vegetation types, followed by GDGT IIa and GDGT IIIa (Fig. 2). GDGT Ib, IIb and Ic occur in minor, GDGT IIc and IIIb only in trace amounts. GDGT IIIc was below the detection limit in most of the samples (Tab. S3). Although other studies document an influence of the vegetation cover on soil temperature and soil water content, which control the microbial community composition in soils (Awe et al., 2015; Liu et al., 2014; Mueller-Niggemann et al., 2016), we find no statistically different pattern of the individual brGDGTs.

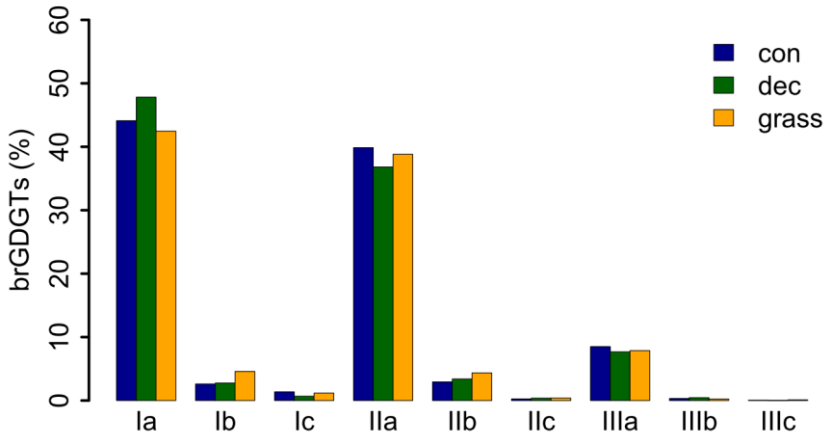

Fig. 2. Mean concentrations of individual brGDGTs as percentage of all brGDGTs for the three investigated types. Abbreviations: con = coniferous forest sites (n=9); dec = deciduous forest sites (n=14); grass = grassland sites (n=6).

Total concentrations of brGDGTs range from 0.32 to 9.17 µg/g dry weight and tend to be highest for the coniferous samples and lowest for the grasses (Fig. 3A, Tab. S3). Bulk brGDGT concentrations lie within the range of other studies examining soils of mid latitude regions (Huguet et al., 2010b, 2010a; Weijers et al., 2011). Similar concentrations in coniferous and deciduous samples imply that brGDGT production does not strongly vary in soils below different forest types. The grass samples show lower brGDGT concentrations compared to the forest samples, but this is probably mainly due to ploughing of the grass sites in former times and hence admixing of mineral subsoil material. The differences in brGDGT concentrations are not significant (p-value = 0.06).

3.2 BIT index

Most of the samples have a BIT index higher than 0.9 (Fig 3B and Tab. S3). The BIT-values are typical for soils in humid and temperate climate regions (Weijers et al., 2006). However,

outliers exist. The most likely source of iGDGTs in soils are Thaumarchaeota, i.e. aerobe ammonia oxidizing archaea producing Crenarchaeol and its regioisomer (Schouten et al., 2013 and references therein), when precipitation amount drops below 700-800 mm (Dang et al., 2016; Dirghangi et al., 2013). The P_{MA} data of our sampling sites mostly show precipitation > 550 mm (Fig. 1B), but one has to be aware that this data is based on the climate station nearest to the respective sampling locations and microclimate effects, such as sunlight exposure, canopy cover or exposition might have a pronounced influence on the brGDGT vs. iGDGT distribution. Mueller-Niggemann et al. (2016) found higher BIT indices in upland soils compared to paddy soils and stated that the management type also influences BIT values in soils. Along our transect, grass sites tend to have slightly lower BIT-values than forest sites, probably due to the absence of a litter layer and hence, no isolation mechanism preventing evaporation of soil water. Differences between vegetation types are not significant (p-value = 0.32).

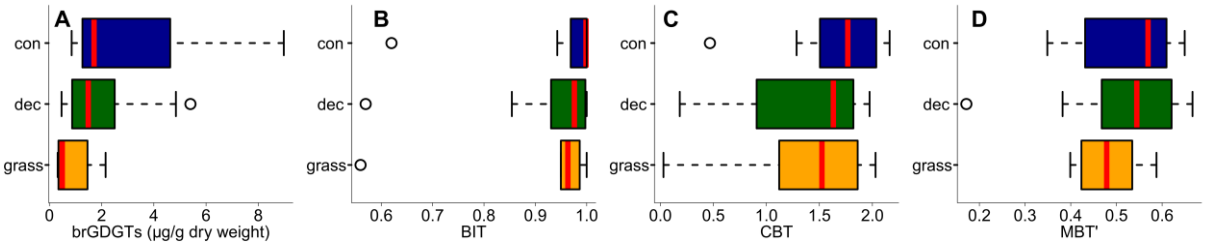

Fig. 3. (A) Total concentrations of brGDGTs in µg g^{-1} dry weight, as well as (B) BIT, (C) CBT and (D) MBT'. Abbreviations: con = coniferous forest sites (n=9); dec = deciduous forest sites (n=14); grass = grassland sites (n=6). Box plots show median (red line), interquartile range (IQR) with upper (75%) and lower (25%) quartiles, lowest whisker still within 1.5IQR of lower quartile, and highest whisker still within 1.5IQR of upper quartile, dots mark outliers.

3.3 CBT-derived pH

The CBT ratio shows a pronounced variation independent of vegetation type with values between 0.03 and 2.16 (Fig 3C). The coniferous samples tend to be highest, but the differences between vegetation types are not significant (p-value = 0.48). The CBT index can be related to pH in acidic and/or humid soils (e.g. Dirghangi et al., 2013; Mueller-Niggemann et al., 2016; Peterse et al., 2012; Weijers et al., 2007) but might be an indicator of soil water content and hence, precipitation in more arid and alkaline soils (e.g. Dang et al., 2016). There is a pronounced correlation between CBT and soil pH (Fig. 4), which is in good agreement with other studies from mid latitude regions where precipitation is relatively high (Anderson et al., 2014 and references therein). Moreover, the CBT to pH relationship in terms of slope and intersect in our dataset (CBT = -0.47 × pH + 3.5, r^2 = 0.7, p-value < 0.0001, n = 29) is well comparable to the correlation described for the global calibration dataset of Peterse et al. (2012) (CBT = -0.36 × pH + 3.1, r^2 = 0.7, p-value < 0.0001, n = 176).

However, there are some outliers in the CBT-pH correlation, which need a further examination (see locations grass L04, dec L10 and dec L12 as marked in Figs. 4 and 5). The outliers show lower BIT indices (< 0.85, Tab. S3). Even though the data from the nearest climate station suggest no abnormal P_{MA}. Local effects such as differences in the amount of sunlight exposure, nutrient availability for brGDGT producing organisms or, most likely soil water content might

influence the brGDGT production at these locations (Anderson et al., 2014; Dang et al., 2016). A lower BIT index as well as a lower CBT occur when soil water content decreases (Dang et al., 2016; Sun et al., 2016) or when aeration is high and less anoxic microhabitats for GDGT producing microbes exist (e.g. Dirghangi et al., 2013).

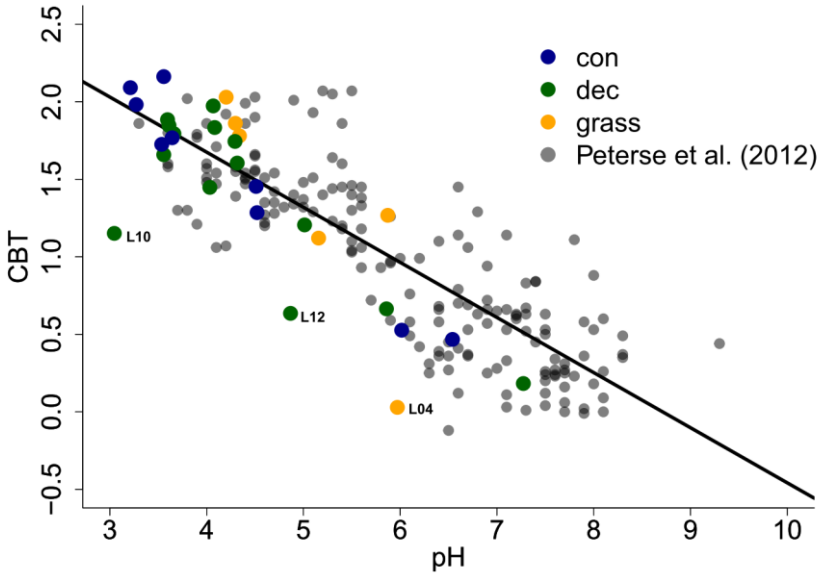

Fig. 4. CBT to pH relationship in our dataset in comparison to the global calibration dataset from Peterse et al. (2012) (CBT = -0.36 × pH + 3.1, r^2 = 0.7, p-value < 0.0001, n = 176, black line). Abbreviations: con = coniferous forest sites (n=9); dec = deciduous forest sites (n=14); grass = grassland sites (n=6).

As the CBT and pH are similarly correlated in our dataset and the global dataset of Peterse et al. (2012), the CBT-derived pH correlated well with the actual pH (Fig. 5A; R^2 = 0.3). Expressed as ΔpH (CBT-derived pH - measured pH), there is a tendency that the GDGTs result in an overestimation of the real pH for the forest sites (Fig. B). Yet a Kruskal-Wallis test shows no statistically significant difference between the vegetation types, with a p-value of 0.13. The overall ΔpH of 0.6 ±0.6 shows that the reconstruction of soil pH using brGDGTs works well along this transect.

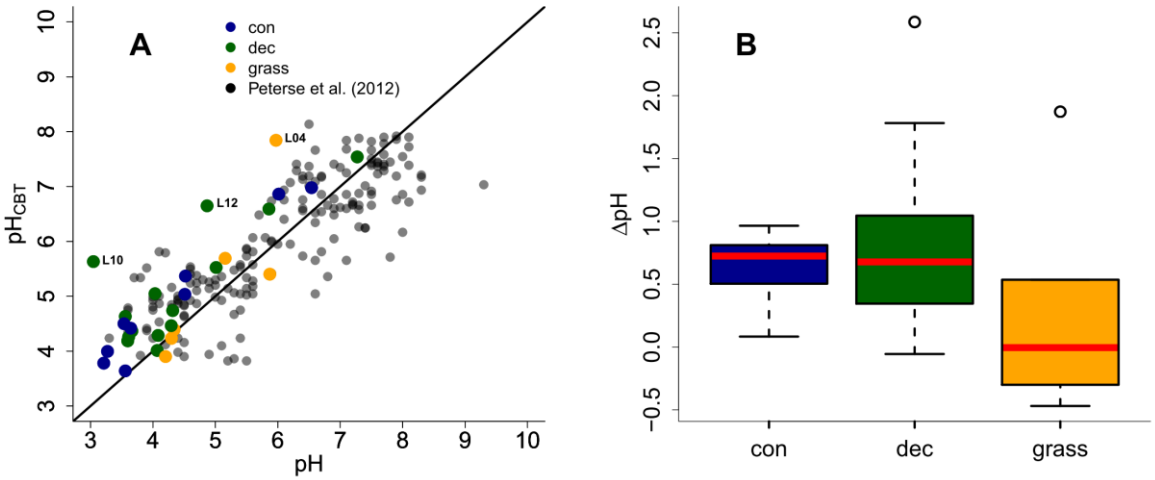

Fig. 5. (A) Correlation between measured pH and reconstructed soil pH (pH_{CBT}) from our transect data in comparison to the global calibration dataset from Peterse et al. (2012) (R^2 = 0.7, RMSE = 0.75, n = 176). Black line indicates the 1:1 relationship. (B) Boxplots of ΔpH (refers to pH_{CBT}-pH). Box plots show median (red line), interquartile range (IQR) with upper (75%) and lower (25%) quartiles, lowest whisker still within 1.5IQR of lower quartile, and highest whisker still within 1.5IQR of upper quartile, dots mark outliers. Abbreviations: con = coniferous forest sites (n=9); dec = deciduous forest sites (n=14); grass = grassland sites (n=6).

3.4 MBT'-CBT-derived T_{MA} reconstructions

The MBT' shows high variability with values ranging from 0.17 to 0.67 no statistical differences between vegetation types (p-value = 0.54; Fig. 3D, Tab. S3). When comparing reconstructed (MBT'-CBT-derived) T_{MA} with climate station T_{MA}, the data plot close to the 1:1 line, and fit well into the global dataset of Peterse et al. (2012) (Fig. 6A). The ΔT_{MA} reveal an overall offset of 0.5°C ±2.4 and there is no statistically difference between vegetation types (Fig. 6B). The standard deviation in ΔT_{MA} of ±2.4 is well in line with the RMSE of 5.0 for the global calibration dataset (Peterse et al., 2012).

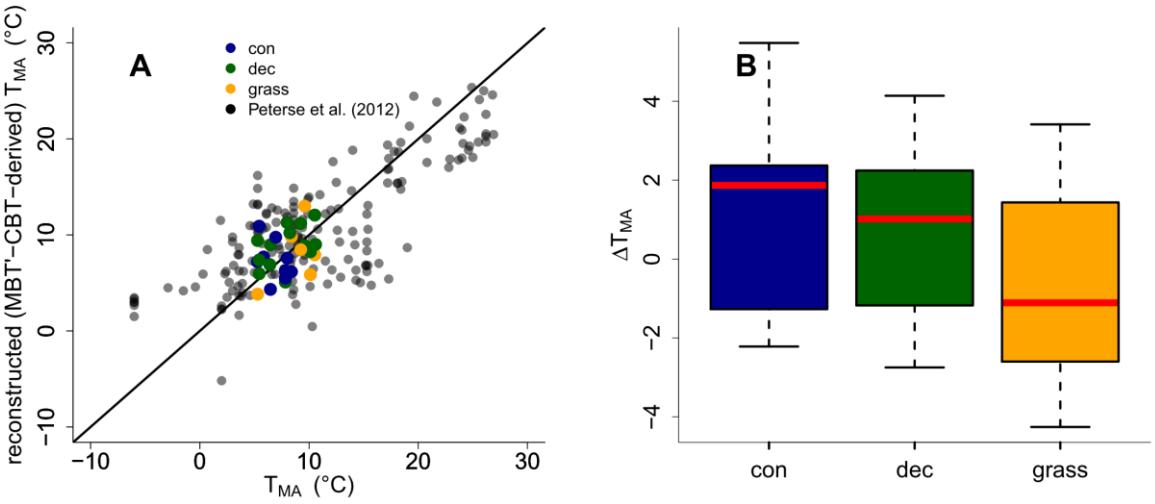

Fig. 6. (A) Correlation between climate station T_{MA} and reconstructed (MBT'-CBT-derived) T_{MA}. For comparison, the global calibration dataset from Peterse et al. (2012) is shown. The black line indicates the 1:1 relationship. (B) Boxplots of ΔT_{MA} (refers to reconstructed T_{MA}-T_{MA} from climate stations) in the different vegetation types from our transect study. Box plots show median (red line), interquartile range (IQR) with upper (75%) and lower (25%) quartiles, lowest whisker still within 1.5IQR of lower quartile, and highest whisker still within 1.5IQR of upper quartile, dots mark outliers. Abbreviations: con = coniferous forest sites (n=9); dec = deciduous forest sites (n=14); grass = grassland sites (n=6).

3.5 Potential impact of the used liquid chromatography method on pH and T_{MA} reconstructions

The GDGT data presented in this study are not acquired on the up-to-date method (e.g. compare De Jonge et al., 2014 vs. Zech et al., 2012c). De Jonge et al. (2014) presented a new liquid chromatography method which enables the separation for the brGDGTs with m/z 1036, 1034

and 1032, 1050, 1048 and 1046 into 6-methyl and 5-methyl stereoisomers. The old method did not allow such a separation (Zech et al., 2012c), thus in the calibration often the sum of 6 and 5-methlyted brGDGTs was used (see and compare De Jonge et al., 2014 vs. Peterse et al., 2012). This introduce scatter to the MBT'-CBT-based T_{MA} reconstructions and can cause a correlation between pH and MBT' (for more details see De Jonge et al., 2014). De Jonge et al. (2014) moreover show that the 6-methyl brGDGTs are ubiquitous abundant in soils from all over the world, based on reanalysing the dataset of Peterse et al. (2012). However, they also compare reconstructed T_{MA} values based MBT'-CBT calibration (Peterse et al., 2012) and their new developed T_{MA} calibration and state that they plot around a 1:1 line. They furthermore state, that especially for arid areas larger deviations can be expected. Finally, they conclude that the use of the new developed calibrations will improve the T_{MA} and pH reconstructions for areas with arid climate conditions. Because our study transect spans form southern Germany to southern Sweden, representing temperate and humid climate conditions, we argue that the usage of the older liquid chromatorgraphy method do not introduce a systematic error in our T_{MA} and pH reconstructions. Still, a higher variability/scatter could be associated with the calibration of Peterse et al. (2012) and therefore also present in our T_{MA} and pH reconstructions.

3.6 Apparent fractionation of δ^2H and $\delta^{18}O$ in the different vegetation types

The δ^2H values could be obtained for *n*-alkanes C_{27}, C_{29} and C_{31} in all samples and additionally at two locations for *n*-C_{25} and *n*-C_{33} at six other locations. The $\delta^2H_{n\text{-alkane}}$ values, calculated as mean of *n*-C_{25} to *n*-C_{31} δ^2H, ranges from -156 to -216‰. Pooled standard deviations show an overall average of 3.6‰. The $\delta^{18}O_{sugar}$ values, calculated as the area weighted means for arabinose and xylose, ranges from 27.7 to 39.4‰. The average weighted mean standard deviation is 1.4‰. The compound-specific isotope data is summarized along with the calculations in Tab. S4.

Apparent fractionation ($\varepsilon_{n\text{-alkane/precipitation}}$) is on the order of -120 to -150‰, i.e. a bit less than the biosynthetic fraction of -160‰. This implies that evapotranspirative enrichment is ~ 10 to 40‰ (Fig. 7A). $\varepsilon_{n\text{-alkane/precipitation}}$ is lower for grass sites compared to the forest sites. Differences are significant between deciduous and grass sites (p-value = 0.005). This finding supports the results of other studies (Kahmen et al., 2013; Liu and Yang, 2008; McInerney et al., 2011), and can be named "signal damping". Grasses do not only incorporate the evaporatively-enriched leaf water only but also unenriched xylem water in the growth and differentiation zone of grasses (Gamarra et al., 2016; Liu et al., 2017).

The grass-derived hemicellulose sugar biomarkers do not fully record the evapotranspirative enrichment of the leaf water, either, as indicated by lower apparent fractionation ($\varepsilon_{sugar/precipitation}$) in Fig. 7B. The differences are significant between forest and grass sites (p-value < 0.005). This is in agreement with a study on cellulose extracted from grass blades (Helliker and Ehleringer, 2002), and again, the "signal damping" can be explained with incorporation of enriched leaf water and non-enriched stem water.

Based on the comparison of evapotranspirative enrichment between forest and grass sites, the "signal damping" can be quantified to be ~ 31% for the hemicellulose sugars, and ~ 49% for the *n*-alkanes. This is in agreement with other studies that reported a loss of 22% of the leaf

water enrichment for hemicellulose sugars (Helliker and Ehleringer, 2002) and 39 to 62% loss of the leaf water enrichment for *n*-alkanes (Gamarra et al., 2016).

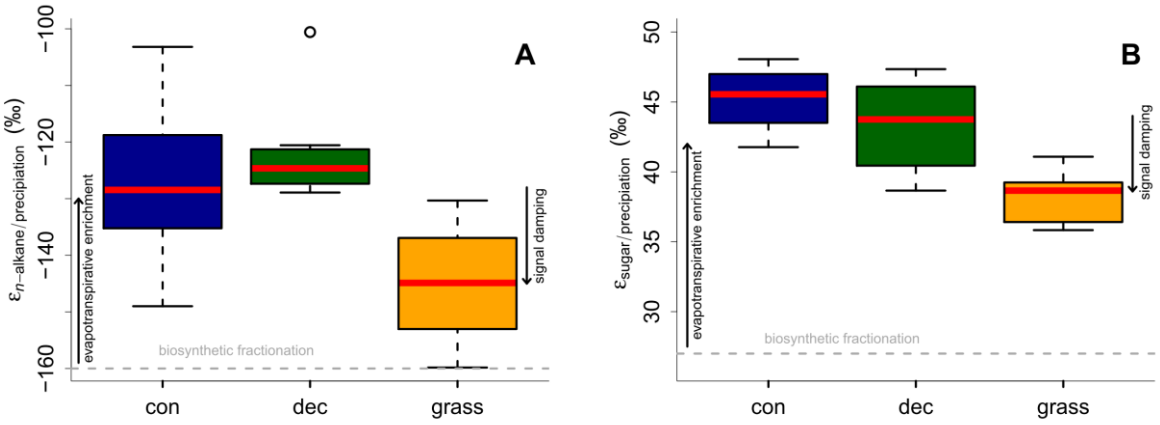

Fig. 7. Apparent fractionation (A) $\varepsilon_{n\text{-alkane/precipitation}}$ and (B) $\varepsilon_{sugar/precipitation}$. Biosynthetic fractionation factors according to section 2.4.2. Box plots show median (red line), interquartile range (IQR) with upper (75%) and lower (25%) quartiles, lowest whisker still within 1.5IQR of lower quartile, and highest whisker still within 1.5IQR of upper quartile, dots mark outliers. Abbreviations: con = coniferous forest sites (n=9); dec = deciduous forest sites (n=11 and 14 for *n*-alkanes and sugars, respectively); grass = grassland sites (n=4 and 6 for *n*-alkanes and sugars, respectively). The figure conceptually illustrates the effect of biosynthetic fractionation and evapotranspirative enrichment as well as "signal damping".

3.7 $\delta^2H_{source\text{-}water}$ and $\delta^{18}O_{source\text{-}water}$ reconstructions

The δ^2H versus $\delta^{18}O$ diagram shown in Fig. 8 graphically illustrates the reconstruction of $\delta^2H_{leaf\text{-}water}$ and $\delta^{18}O_{leaf\text{-}water}$ (colored dots) from $\delta^2H_{n\text{-alkane}}$ and $\delta^{18}O_{sugar}$ (crosses), as well as the reconstruction of $\delta^2H_{source\text{-}water}$ and $\delta^{18}O_{source\text{-}water}$ (black dots). For reconstructing $\delta^2H_{source\text{-}water}$ and $\delta^{18}O_{source\text{-}water}$, LELs with an average slope of 2.8 ±0.1 (Eq. 10) can be generated through every leaf water point and the intercepts of these LELs with the GMWL.

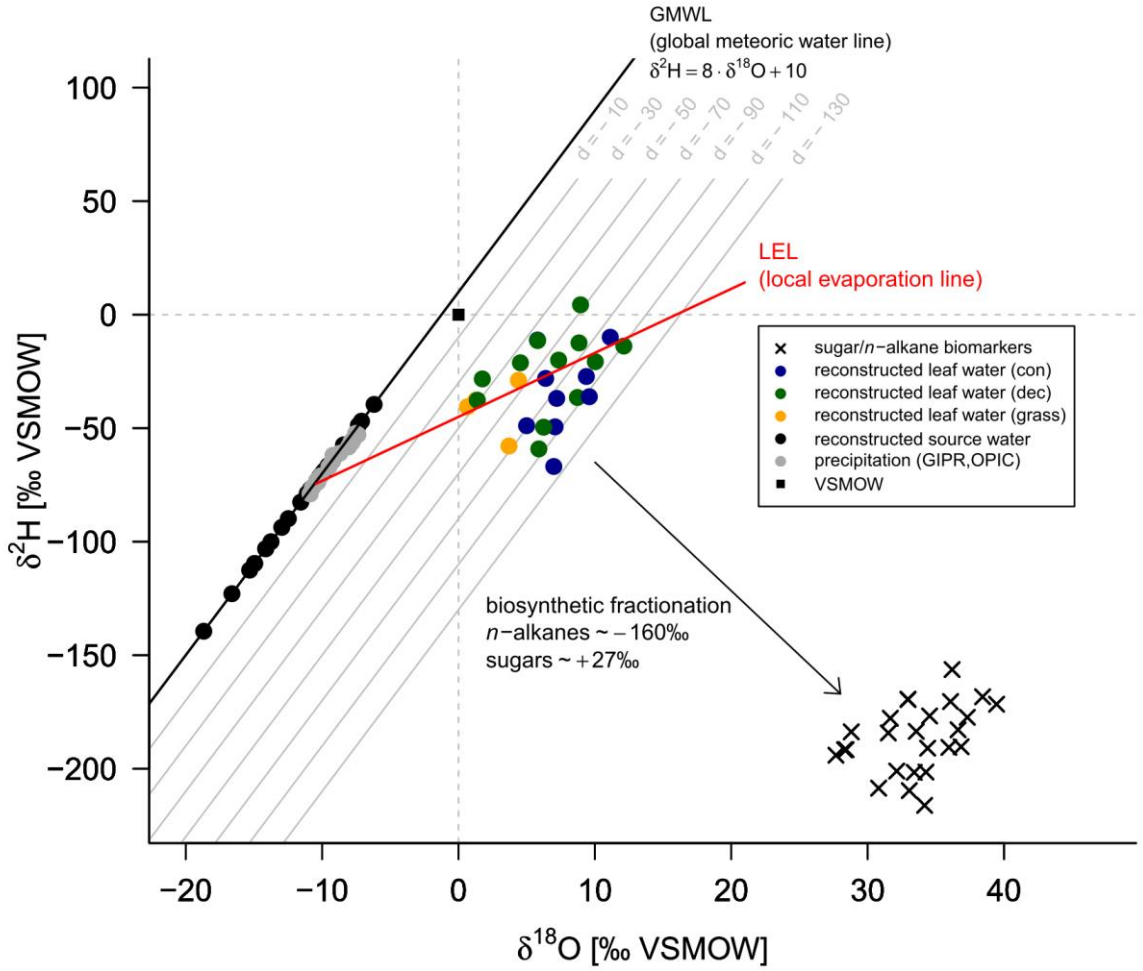

Fig. 8. δ^2H vs. $\delta^{18}O$ diagram illustrating the coupled $\delta^2H_{n\text{-alkane}}$-$\delta^{18}O_{sugar}$ approach: measured $\delta^2H_{n\text{-alkane}}$ and $\delta^{18}O_{sugar}$ values, reconstructed $\delta^2H_{leaf\text{-}water}$ and $\delta^{18}O_{leaf\text{-}water}$ (according Eqs. 8 and 9) and reconstructed $\delta^2H_{source\text{-}water}$ and $\delta^{18}O_{source\text{-}water}$ in comparison to GIPR and OIPC-based $\delta^2H_{precipitation}$ and $\delta^{18}O_{precipitation}$. Abbreviations: con = coniferous forest sites (n=9); dec = deciduous forest sites (n=11); grass = grassland sites (n=4).

The reconstructed $\delta^2H_{source\text{-}water}$ and $\delta^{18}O_{source\text{-}water}$ results can be compared with the $\delta^2H_{GIPR,OIPC}$ and $\delta^{18}O_{GIPR,OIPC}$ data (Fig. 9). This comparison reveals that the coupled $\delta^2H_{n\text{-alkane}}$-$\delta^{18}O_{sugar}$ approach yields more accurate $\delta^2H_{source\text{-}water}$ and $\delta^{18}O_{source\text{-}water}$ compared to single $\delta^2H_{n\text{-alkane}}$ approaches. However, the range of the reconstructed $\delta^2H_{source\text{-}water}$ and $\delta^{18}O_{source\text{-}water}$ values is clearly larger than in $\delta^2H_{GIPR,OIPC}$ and $\delta^{18}O_{GIPR,OIPC}$ values. δ^2H is systematically underestimated by ~ 21‰ ±22 (Fig. 9B) and $\delta^{18}O$ by ~ 2.9‰ ±2.8 (Fig. 9D). The type of vegetation seems to be not particularly relevant (p-value = 0.18 for $\Delta\delta^2H$ and p-value = 0.34 for $\Delta\delta^{18}O$). Nevertheless, the systematic offsets tend to be lowest for the decidous sites ($\Delta\delta^2H$ and $\Delta\delta^{18}O$ is closer to zero with ~-5‰ ±15 and ~-1.1‰ ±2.1), followed by grass sites (~-14‰ ±20 and ~-2.1‰ ±2.6). In comparison, the coniferous sites show the largest offsets (~-23‰ ±26 for $\Delta\delta^2H$ ~-3.0‰ ±3.3 for $\Delta\delta^{18}O$). Differences are, however, not statistically significant. The systematic offset and the large variability might have more specific reasons, and we suggest that this is related to the type of vegetation. Deciduous trees produce lots of leaf waxes and sugars (e.g. Prietzel et al., 2013; Zech et al., 2012a), and all biomarkers reflect and record the

evapotranspirative enrichment of the leaf water (e.g. Kahmen et al., 2013; Tuthorn et al., 2014). However, coniferous trees produce quite low amounts of *n*-alkanes (Diefendorf and Freimuth, 2016; Zech et al., 2012a), while sugar concentrations are as high as in other vascular plants (e.g. Hepp et al., 2016; Prietzel et al., 2013). For the coniferous soil samples this means that the *n*-alkanes stem most likely from the understory whereas the sugars originate from grasses and coniferous needles. When the understory is dominated by grass species then the *n*-alkane biomarkers do not record the full leaf water enrichment signal, whereas the sugars from the needles do. The reconstructed leaf water for the coniferous sites is therefore too negative concerning δ^2H, and reconstructed $\delta^2H_{source\text{-}water}$ and $\delta^{18}O_{source\text{-}water}$ values thus also become too negative (Fig. 8). Concerning the grass sites the following explanation can be found. Correcting for "signal damping" makes the reconstructed leaf water points more positive and shifts them in Fig. 8 up and right. As the "signal damping" is stronger for δ^2H than for $\delta^{18}O$ the corrected leaf water points would now above the uncorrected ones. The corrected leaf water points leads to more positive reconstructed $\delta^2H_{source\text{-}water}$ and $\delta^{18}O_{source\text{-}water}$ values for the grass sites. However, Gao et al. (2014) and Liu et al. (2016) showed that the ε_{bio} of monocotyledon plants could larger than those of dicotyledonous once. This would therefore course a more negative apparent fractionation factor for grasses compared to trees. We observe that the apparent fractionation is indeed more negative for the grass sites compared to the forest sites. The effects of "signal damping" vs. variable ε_{bio} along with vegetation types are indistinguishable here. As an outlook for a future study, we therefore strongly recommend a comparison between the here measured $\delta^2H_{n\text{-}alkane}$ values with modelled once using a new available model approach from Konecky et al. (2019), which could provide insights if such vegetation effects on ε_{bio} of ^2H in *n*-alkanes are describable.

Vegetation type specific rooting depths could partly cause the overall high variability in reconstructed $\delta^2H_{source\text{-}water}$ and $\delta^{18}O_{source\text{-}water}$. Deep rooting species most likely use the water from deeper soil horizons and/or shallow ground water, which is equal to the (weighted) mean annual precipitation (e.g. Herrmann et al., 1987). Shallow rooting plants take up water from upper soil horizons, which is influenced by seasonal variations in $\delta^2H_{precipiation}$ and $\delta^{18}O_{precipiation}$ and by soil water enrichment (Dubbert et al., 2013). Thus, the overall assumption that the source water of the plants reflects the local (weighted) mean precipitation might be not fully valid for all sites. Moreover, a partly contribution of root-derived rather than leaf-derived sugar biomarkers in our topsoil samples is very likely. This does, by contrast, not apply for *n*-alkanes, which are hardly produced in roots (Zech et al., 2012b and the discussion therein).

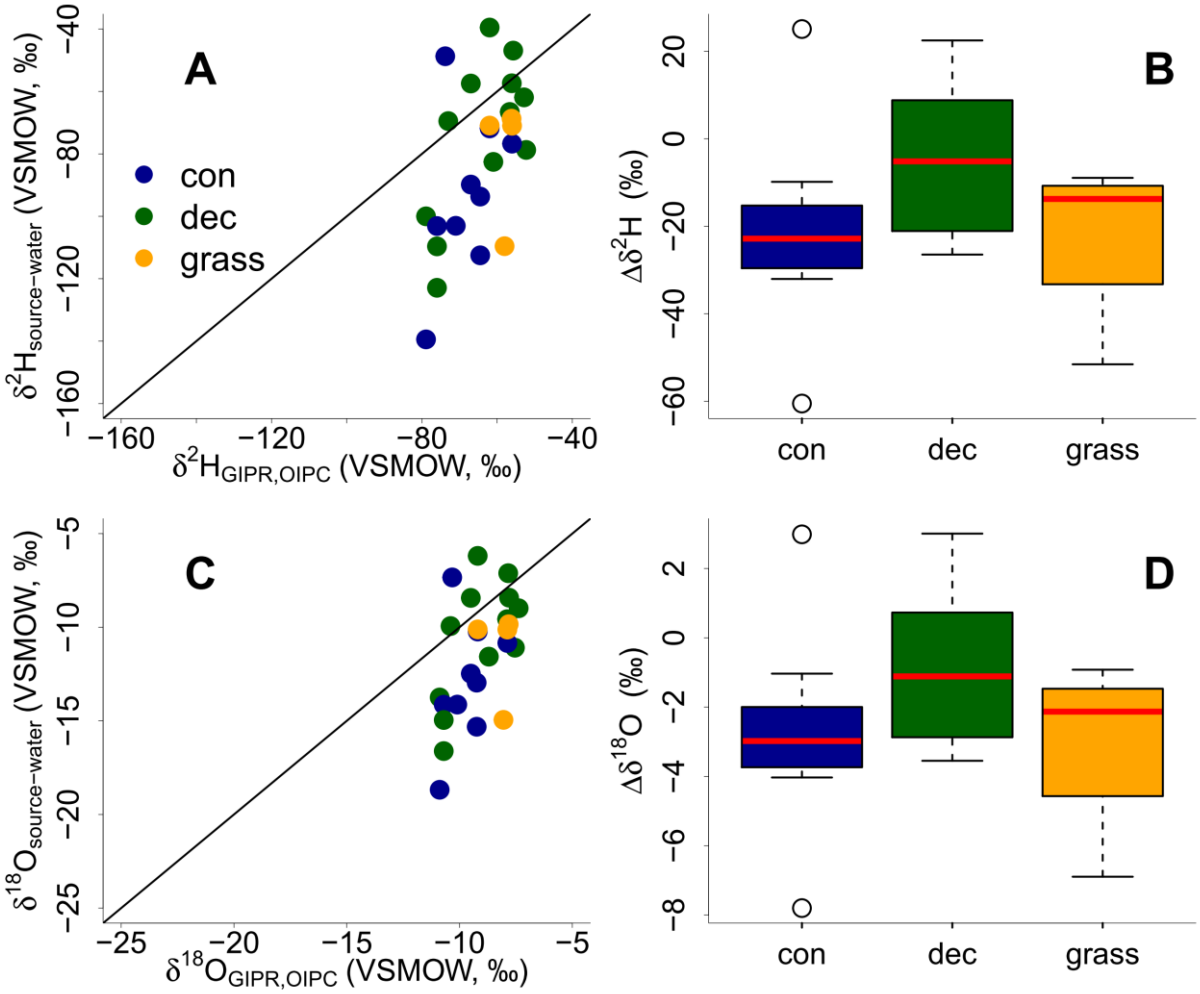

Fig. 9. Correlation of reconstructed $\delta^2H_{source-water}$ and $\delta^{18}O_{source-water}$ vs. precipitation $\delta^2H_{GIPR,OIPC}$ and $\delta^{18}O_{GIPR,OIPC}$ (A and C). Black lines indicate 1:1 relationship. Differences between reconstructed source water and precipitation ($\Delta\delta^2H,\delta^{18}O$ = $\delta^2H_{source-water},\delta^{18}O_{source-water}$ - $\delta^2H_{GIPR,OIPC},\delta^{18}O_{GIPR,OIPC}$) for the three different vegetation types (B and D). Box plots show median (red line), interquartile range (IQR) with upper (75%) and lower (25%) quartiles, lowest whisker still within 1.5IQR of lower quartile, and highest whisker still within 1.5IQR of upper quartile. Abbreviations: con = coniferous forest sites (n=9); dec = deciduous forest sites (n=11); grass = grassland sites (n=4).

Moreover, the high variability within the vegetation types could be caused by variability in ε_{bio} of ^2H in *n*-alkanes, as well as ^{18}O in sugars. There is an ongoing discussion about the correct ε_{bio} for ^{18}O in hemicellulose sugars (Sternberg, 2014 vs. Zech et al., 2014), and ε_{bio} is probably not constant over all vegetation types. This translates into errors concerning leaf water reconstruction and thus for reconstructing $\delta^2H_{source-water}$ and $\delta^{18}O_{source-water}$ values (Eq. 9 and Fig. 8). Likewise, the ε_{bio} values reported in the literature for ^2H of *n*-alkanes can be off from -160‰ by tens of permille (Feakins and Sessions, 2010; Tipple et al., 2015; Feakins et al., 2016; Freimuth et al., 2017). The degree to which hydrogen originates from NADPH rather than leaf water is important, because NADPH is more negative (Schmidt et al., 2003). The wide range in biosynthetic ^2H fractionation factors, which can be even larger, is therefore also related to the carbon and energy metabolism state of plants (Cormier et al., 2018).

3.8 RH reconstruction

Reconstructed RH_{MDV} ranges from 34 to 74%, while RH_{MDV} from climate station data range from 61 to 78% (Fig. 10A). Biomarker-based values thus systematically underestimate the station data (ΔRH_{MDV} = -17% ±12). Yet the offsets are much less for deciduous tree and grass sites (ΔRH_{MDV} = -10% ±12 and -7% ±9, respectively; Fig. 10B). The offsets for the coniferous sites are -30% ±11, and significantly larger than for the deciduous and grass sites (p-values < 0.05).

Too low reconstructed RH_{MDV} values for the coniferous sites make sense in view of the previously discussed option that soils contain *n*-alkanes from the understory (which is dominated by grass species), while sugars stem from needles and grasses. As explained earlier already, the "signal damping" leads to too negative reconstructed $\delta^2H_{leaf\text{-}water}$ (whereas $\delta^{18}O$ is affected less by the "signal damping"), and too negative $\delta^2H_{leaf\text{-}water}$ translates into overestimated d-excess and underestimated RH values. In Fig. 8, a correction for this require moving the coniferous leaf water data points upwards towards more positive δ^2H values, thus the distance between the leaf water and the source water is reduced. It should be noted that also here variable ε_{bio} along with vegetation types could not be distinguished from "signal damping" effects.

The underestimation of RH for the deciduous and grass sites could be partly associated with the use of the GMWL as baseline for the coupled $\delta^2H_{n\text{-}alkane}$-$\delta^{18}O_{sugar}$ approach. The deuterium-excess of the LMWLs is generally lower than the +10‰ of the GMWL, while the slopes of the LMWLs are well comparable to the GMWL (Stumpp et al., 2014). In addition, if soil water evaporation occurred before water uptake by the plants, this would lead to an underestimation of biomarker-based RH_{MDV} values. It can be furthermore assumed that plant metabolism is highest during times with direct sunshine and high irradiation, i.e. during noon at sunny days. The relevant RH could therefore be lower than the climate station-derived RH_{MDV}. Indeed, already climate station RH_{MDV} is considerable lower than RH_{MA} and RH_{MV} (Tab. S1).

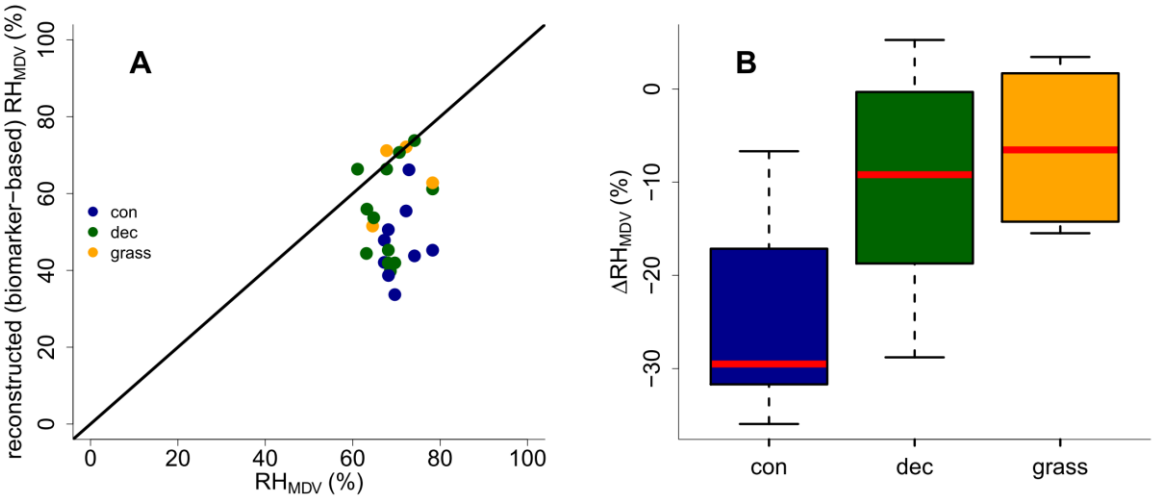

Fig. 10. (A) Comparison of reconstructed (biomarker-based) RH_{MDV} values and climate station RH_{MDV} data. The black line indicates the 1:1 relationship. (B) Differences between reconstructed and climate station RH_{MDV} values (ΔRH_{MDV} = reconstructed – climate station RH_{MDV}) for the three different vegetation types along the transect. Abbreviations: con = coniferous forest sites (n=9); dec = deciduous forest sites (n=11); grass = grassland sites (n=4).

The uncertainty of reconstructed RH_{MDV} values are large for all three investigated vegetation types, and again these uncertainties are probably also related to ε_{bio}, which is most likely not constant as assumed for our calculations. Moreover, microclimate variability is underestimated in our approach. As mentioned in sections 2.4.2 and 3.7, in the coupled approach not only the source water of the plants is equated with (weighted) mean annual precipitation, but also an isotopic equilibrium between the source water and the (local) atmospheric water vapour is assumed. However, in areas with distinct seasonality this might be not fully valid. To account for this lack of equilibrium between precipitation and local atmospheric water vapour, apparent ε values can be calculated with data from Jacob and Sonntag, (1991). As shown by Hepp et al. (2018) those values can be used to achieve alternative RH reconstructions based on the coupled $\delta^2H_{n\text{-alkane}}$-$\delta^{18}O_{sugar}$ approach. Such calculated RH_{MDV} values are on average 1.5% more negative than the original values. However, this difference in RH is far below the analytical uncertainties of the compound-specific biomarker isotope analysis.

Finally, the integration time of the investigated topsoils has to be discussed. Unfortunately, no ^{14}C dates are available for the soil samples. However, most likely the organic matter has been built up over a longer timescale than the available climate data, which is used for comparison. In combination with vegetation changes/management changes throughout that period, this could surely lead to a less tight relationship of the reconstructions compared to the climate station data. Root input of arabinose and xylose seems to be of minor relevance in our topsoil samples. Otherwise, the reconstructed $\delta^{18}O_{sugar}$ values would be too negative resulting in RH_{MDV} overestimations, which is not observed.

4 Conclusions

We were able to show that

(i) the vegetation type does not significantly influence the brGDGT concentrations and proxies, yet the coniferous sites tend to have higher brGDGT concentrations, BIT indices and CBT-MBT' ratios, while grass sites tend to be lowest.

(ii) CBT faithfully records soil pH with a median ΔpH of 0.6 ±0.6, The CBT overestimates the real pH particularly at the forest sites.

(iii) CBT-MBT'-derived T_{MA} reflect the climate station-derived T_{MA} values with a median ΔT_{MA} of 0.5°C ±2.4, but again slightly too high reconstruction for the forest sites were observed.

(iv) differences in the apparent fractionation between the investigated vegetation types could be caused by "signal damping" or variable ε_{bio}, which are indistinguishable here.

(v) the reconstructed $\delta^2H_{source\text{-}water}$ and $\delta^{18}O_{source\text{-}water}$ reflect the $\delta^2H_{GIPR,OIPC}$ and $\delta^{18}O_{GIPR,OIPC}$ with a systematic offset for δ^2H of ~-21‰ ±22 and for $\delta^{18}O$ of ~-2.9‰ ±2.8 (based on overall medians of $\Delta\delta^2H$, $\delta^{18}O$). This is caused by too negative reconstructions for coniferous and grass sites. For coniferous sites, this can be explained with *n*-alkanes originating from understory grasses. As for the grass sites, the "signal damping" or variable ε_{bio} along with vegetation types more effect δ^2H

than $\delta^{18}O$. This leads to too negative reconstructed $\delta^{2}H_{leaf\text{-}water}$ values and thus to too negative $\delta^{2}H_{source\text{-}water}$ and $\delta^{18}O_{source\text{-}water}$ reconstructions.

(vi) reconstructed (biomarker-based) RH_{MDV} values tend to underestimate climate station-derived RH_{MDV} values (ΔRH_{MDV} = ~ -17% ±12). For coniferous sites the underestimations are strongest, which can be explained with understory grasses being the main source of *n*-alkanes for the investigated soils under coniferous forests.

Overall, our study highlights the great potential of GDGTs and the coupled $\delta^{2}H_{n\text{-}alkane}$-$\delta^{18}O_{sugar}$ approach for more quantitative paleoclimate reconstructions. Taking into account effects of different vegetation types improves correlations and reconstructions. This holds particularly true for the coupled $\delta^{2}H_{n\text{-}alkane}$-$\delta^{18}O_{sugar}$ approach, which is affected by "signal damping" of the grass vegetation or variable ε_{bio} along with vegetation types. By contrast, vegetation-related effects do not strongly influence the brGDGT-derived reconstructions. Assuming constant biosynthetic fractionation is likely a considerable source of uncertainty and should be in focus in future field and/or modelling studies. Climate chamber experiments would be very useful to further evaluate and refine the coupled $\delta^{2}H_{n\text{-}alkane}$-$\delta^{18}O_{sugar}$ approach, because uncertainties related to microclimate variability can be reduced. Field experiments like ours suffer from the fact that biomarker pools in the sampled topsoils may have been affected by past vegetation and climate changes and by the rather small range covered by the sampled transect. Both makes the comparison between reconstructions and observations more difficult compared to large datasets und well defined conditions.

Acknowledgements

We thank L. Wüthrich, H. Veit, T. Sprafke, A. Groos (all University of Bern), A. Kühnel (Technical University of Munich) for constructive discussions and statistical advices, and M. Schaarschmidt (University of Bayreuth), C. Heinrich and M. Benesch (Martin-Luther-University Halle-Wittenberg) for laboratory assistance during $\delta^{18}O_{sugar}$ analysis and pH measurements, respectively. The Swiss National Science Foundation (PP00P2 150590) funded this research. J. Hepp greatly acknowledges the support by the German Federal Environmental Foundation (DBU) in form of his PhD-fellowship.

References

Allison, G. B., Gat, J. R. and Leaney, F. W. J.: The relationship between deuterium and oxygen-18 delta values in leaf water, Chemical Geology, 58, 145–156, 1985.

Amelung, W., Cheshire, M. V. and Guggenberger, G.: Determination of neutral and acidic sugars in soil by capillary gas-liquid chromatography after trifluoroacetic acid hydrolysis, Soil Biology and Biochemistry, 28(12), 1631–1639, 1996.

Anderson, V. J., Shanahan, T. M., Saylor, J. E., Horton, B. K. and Mora, A. R.: Sources of local and regional variability in the MBT'/CBT paleotemperature proxy: Insights from a modern elevation transect across the Eastern Cordillera of Colombia, Organic Geochemistry, 69, 42–51, doi:10.1016/j.orggeochem.2014.01.022, 2014.

644 Awe, G. O., Reichert, J. M. and Wendroth, O. O.: Temporal variability and covariance
645 structures of soil temperature in a sugarcane field under different management practices
646 in southern Brazil, Soil and Tillage Research, 150, 93–106,
647 doi:10.1016/j.still.2015.01.013, 2015.

648 Bariac, T., Gonzalez-Dunia, J., Katerji, N., Béthenod, O., Bertolini, J. M. and Mariotti, A.:
649 Spatial variation of the isotopic composition of water (^{18}O, ^{2}H) in the soil-plant-
650 atmosphere system, 2. Assessment under field conditions, Chemical Geology, 115, 317–
651 333, 1994.

652 Bowen, G. J.: The Online Isotopes in Precipitation Calculator, version 3.1., 2018.

653 Bowen, G. J. and Revenaugh, J.: Interpolating the isotopic composition of modern meteoric
654 precipitation, Water Resources Research, 39(10), 1–13, doi:10.1029/2003WR002086,
655 2003.

656 Brincat, D., Yamada, K., Ishiwatari, R., Uemura, H. and Naraoka, H.: Molecular-isotopic
657 stratigraphy of long-chain *n*-alkanes in Lake Baikal Holocene and glacial age sediments,
658 Organic Geochemistry, 31(4), 287–294, doi:10.1016/S0146-6380(99)00164-3, 2000.

659 Cappelen, J.: Danish Climatological Normals 1971-2000 - for selected stations., 2002.

660 Cernusak, L. A., Wong, S. C. and Farquhar, G. D.: Oxygen isotope composition of phloem sap
661 in relation to leaf water in Ricinus communis, Functional Plant Biology, 30(10), 1059–
662 1070, 2003.

663 Cernusak, L. A., Barbour, M. M., Arndt, S. K., Cheesman, A. W., English, N. B., Feild, T. S.,
664 Helliker, B. R., Holloway-Phillips, M. M., Holtum, J. A. M., Kahmen, A., Mcinerney, F.
665 A., Munksgaard, N. C., Simonin, K. A., Song, X., Stuart-Williams, H., West, J. B. and
666 Farquhar, G. D.: Stable isotopes in leaf water of terrestrial plants, Plant Cell and
667 Environment, 39(5), 1087–1102, doi:10.1111/pce.12703, 2016.

668 Christoph, H., Eglinton, T. I., Zech, W., Sosin, P. and Zech, R.: A 250 ka leaf-wax δD record
669 from a loess section in Darai Kalon , Southern Tajikistan, Quaternary Science Reviews,
670 208, 118–128, doi:10.1016/j.quascirev.2019.01.019, 2019.

671 Coffinet, S., Huguet, A., Anquetil, C., Derenne, S., Pedentchouk, N., Bergonzini, L.,
672 Omuombo, C., Williamson, D., Jones, M., Majule, A. and Wagner, T.: Evaluation of
673 branched GDGTs and leaf wax n-alkane δ^2H as (paleo) environmental proxies in East
674 Africa, Geochimica et Cosmochimica Acta, 198, 182–193,
675 doi:10.1016/j.gca.2016.11.020, 2017.

676 Cormier, M.-A., Werner, R. A., Sauer, P. E., Gröcke, D. R., M.C., L., Wieloch, T., Schleucher,
677 J. and Kahmen, A.: ^{2}H fractiontions during the biosynthesis of carbohydrates and lipids
678 imprint a metabolic signal on the δ^2H values of plant organic compounds, New
679 Phytologist, 218(2), 479–491, doi:10.1111/nph.15016, 2018.

680 Craig, H.: Isotopic Variations in Meteoric Waters, Science, 133, 1702–1703, 1961.

681 Dang, X., Yang, H., Naafs, B. D. A., Pancost, R. D. and Xie, S.: Evidence of moisture control
682 on the methylation of branched glycerol dialkyl glycerol tetraethers in semi-arid and arid
683 soils, Geochimica et Cosmochimica Acta, 189, 24–36, doi:10.1016/j.gca.2016.06.004,
684 2016.

685 Dansgaard, W.: Stable isotopes in precipitation, Tellus, 16(4), 436–468, doi:10.1111/j.2153-
686 3490.1964.tb00181.x, 1964.

687 Dawson, T. E., Mambelli, S., Plamboeck, A. H., Templer, P. H. and Tu, K. P.: Stable Isotopes
688 in Plant Ecology, Annual Review of Ecology and Systematics, 33(1), 507–559,
689 doi:10.1146/annurev.ecolsys.33.020602.095451, 2002.

690 Diefendorf, A. F. and Freimuth, E. J.: Extracting the most from terrestrial plant-derived *n*-alkyl
691 lipids and their carbon isotopes from the sedimentary record: A review, Organic
692 Geochemistry, 103(January), 1–21, doi:10.1016/j.orggeochem.2016.10.016, 2016.

693 Dirghangi, S. S., Pagani, M., Hren, M. T. and Tipple, B. J.: Distribution of glycerol dialkyl
694 glycerol tetraethers in soils from two environmental transects in the USA, Organic
695 Geochemistry, 59, 49–60, doi:10.1016/j.orggeochem.2013.03.009, 2013.

696 Dubbert, M., Cuntz, M., Piayda, A., Maguás, C. and Werner, C.: Partitioning evapotranspiration
697 - Testing the Craig and Gordon model with field measurements of oxygen isotope ratios
698 of evaporative fluxes, Journal of Hydrology, 496, 142–153,
699 doi:10.1016/j.jhydrol.2013.05.033, 2013.

700 DWD Climate Data Center: Historical annual precipitation observations for Germany. [online]
701 Available from: ftp://ftp-
702 cdc.dwd.de/pub/CDC/observations_germany/climate/hourly/precipitation/historical/
703 (Accessed 20 September 2018a), 2018.

704 DWD Climate Data Center: Historical hourly station observations of 2m air temperature and
705 humidity for Germany. [online] Available from: ftp://ftp-
706 cdc.dwd.de/pub/CDC/observations_germany/climate/hourly/air_temperature/historical/
707 (Accessed 19 September 2018b), 2018.

708 Eglinton, T. I. and Eglinton, G.: Molecular proxies for paleoclimatology, Earth and Planetary
709 Science Letters, 275(1), 1–16, 2008.

710 Feakins, S. J. and Sessions, A. L.: Controls on the D/H ratios of plant leaf waxes in an arid
711 ecosystem, Geochimica et Cosmochimica Acta, 74(7), 2128–2141,
712 doi:http://dx.doi.org/10.1016/j.gca.2010.01.016, 2010.

713 Feakins, S. J., Bentley, L. P., Salinas, N., Shenkin, A., Blonder, B., Goldsmith, G. R., Ponton,
714 C., Arvin, L. J., Wu, M. S., Peters, T., West, A. J., Martin, R. E., Enquist, B. J., Asner, G.
715 P. and Malhi, Y.: Plant leaf wax biomarkers capture gradients in hydrogen isotopes of
716 precipitation from the Andes and Amazon, Geochimica et Cosmochimica Acta, 182, 155–
717 172, doi:10.1016/j.gca.2016.03.018, 2016.

718 Freimuth, E. J., Diefendorf, A. F. and Lowell, T. V.: Hydrogen isotopes of *n*-alkanes and *n*-
719 alkanoic acids as tracers of precipitation in a temperate forest and implications for
720 paleorecords, Geochimica et Cosmochimica Acta, 206, 166–183,
721 doi:10.1016/j.gca.2017.02.027, 2017.

722 Frich, P., Rosenørn, S., Madsen, H. and Jensen, J. J.: Observed Precipitation in Denmark, 1961-
723 90., 1997.

724 Gamarra, B., Sachse, D. and Kahmen, A.: Effects of leaf water evaporative ^{2}H-enrichment and
725 biosynthetic fractionation on leaf wax *n*-alkane δ^{2}H values in C3 and C4 grasses, Plant,
726 Cell and Environment Environment, 39, 2390–2403, doi:10.1111/pce.12789, 2016.

727 Gat, J. R.: Comments on the Stable Isotope Method in Regional Groundwater Investigations,
728 Water Resources Research, 7(4), 980–993, doi:10.1029/WR007i004p00980, 1971.

729 van Geldern, R., Baier, A., Subert, H. L., Kowol, S., Balk, L. and Barth, J. A. C.: (Table S1)

730 Stable isotope composition of precipitation sampled at Erlangen, Germany between 2010
731 and 2013 for station GeoZentrum located at Erlangen city center, in In supplement to: van
732 Geldern, R et al. (2014): Pleistocene paleo-groundwater as a pristine fresh water resource
733 in southern Germany – evidence from stable and radiogenic isotopes. Science of the Total
734 Environment, 496, 107-115, https://doi.org/10.1016/j., PANGAEA., 2014.

735 Guggenberger, G., Christensen, B. T. and Zech, W.: Land-use effects on the composition of
736 organic matter in particle-size separates of soil: I. Lignin and carbohydrate signature,
737 European Journal of Soil Science, 45(December), 449–458, 1994.

738 Helliker, B. R. and Ehleringer, J. R.: Grass blades as tree rings: environmentally induced
739 changes in the oxygen isotope ratio of cellulose along the length of grass blades, New
740 Phytologist, 155, 417–424, 2002.

741 Hepp, J., Rabus, M., Anhäuser, T., Bromm, T., Laforsch, C., Sirocko, F., Glaser, B. and Zech,
742 M.: A sugar biomarker proxy for assessing terrestrial versus aquatic sedimentary input,
743 Organic Geochemistry, 98, 98–104, doi:10.1016/j.orggeochem.2016.05.012, 2016.

744 Hepp, J., Wüthrich, L., Bromm, T., Bliedtner, M., Schäfer, I. K., Glaser, B., Rozanski, K.,
745 Sirocko, F., Zech, R. and Zech, M.: How dry was the Younger Dryas? Evidence from a
746 coupled δ^2H-δ^{18}O biomarker paleohygrometer, applied to the Lake Gemündener Maar
747 sediments, Western Eifel, Germany, Climate of the Past Discussions, (September), 1–44,
748 doi:10.5194/cp-2018-114, 2018.

749 Herrmann, A., Maloszewski, P. and Stichler, W.: Changes of ^{18}O contents of precipitation water
750 during seepage in the unsaturated zone, in Proceedings of International Symposium on
751 Groundwater Monitoring and Management, 23 - 28 March, p. 22, Institut of Water
752 Management Berlin (GDR) with support of UNESCO, Dresden., 1987.

753 Hopmans, E. C., Weijers, J. W. H., Schefuß, E., Herfort, L., Sinninghe Damsté, J. S. and
754 Schouten, S.: A novel proxy for terrestrial organic matter in sediments based on branched
755 and isoprenoid tetraether lipids, Earth and Planetary Science Letters, 224(1–2), 107–116,
756 doi:10.1016/j.epsl.2004.05.012, 2004.

757 Horita, J. and Wesolowski, D. J.: Liquid-vapor fractionation of oxygen and hydrogen isotopes
758 of water from the freezing to the critical temperature, Geochimica et Cosmochimica Acta,
759 58(16), 3425–3437, doi:http://dx.doi.org/10.1016/0016-7037(94)90096-5, 1994.

760 Hothorn, T., Bühlmann, P., Dudoit, S., Molinaro, A. and Van Der Laan, M. J.: Survival
761 ensembles, Biostatistics, 7(3), 355–373, doi:10.1093/biostatistics/kxj011, 2006.

762 Hou, J., D'Andrea, W. J. and Huang, Y.: Can sedimentary leaf waxes record D/H ratios of
763 continental precipitation? Field, model, and experimental assessments, Geochimica et
764 Cosmochimica Acta, 72, 3503–3517, doi:10.1016/j.gca.2008.04.030, 2008.

765 Huguet, A., Fosse, C., Metzger, P., Fritsch, E. and Derenne, S.: Occurrence and distribution of
766 extractable glycerol dialkyl glycerol tetraethers in podzols, Organic Geochemistry, 41(3),
767 291–301, doi:10.1016/j.orggeochem.2009.10.007, 2010a.

768 Huguet, A., Fosse, C., Laggoun-Défarge, F., Toussaint, M. L. and Derenne, S.: Occurrence and
769 distribution of glycerol dialkyl glycerol tetraethers in a French peat bog, Organic
770 Geochemistry, 41(6), 559–572, doi:10.1016/j.orggeochem.2010.02.015, 2010b.

771 IAEA/WMO: Global Network of Isotopes in Precipitation. The GNIP Database., 2015.

772 IAEA/WMO: Global Network of Isotopes in Precipitation. The GNIP Database., 2018.

Jacob, H. and Sonntag, C.: An 8-year record of the seasonal- variation of ^{2}H and ^{18}O in atmospheric water vapor and precipitation at Heidelberg, Tellus, 43B(3), 291–300, 1991.

De Jonge, C., Hopmans, E. C., Zell, C. I., Kim, J. H., Schouten, S. and Sinninghe Damsté, J. S.: Occurrence and abundance of 6-methyl branched glycerol dialkyl glycerol tetraethers in soils: Implications for palaeoclimate reconstruction, Geochimica et Cosmochimica Acta, 141, 97–112, doi:10.1016/j.gca.2016.03.038, 2014.

Kahmen, A., Schefuß, E. and Sachse, D.: Leaf water deuterium enrichment shapes leaf wax *n*-alkane δD values of angiosperm plants I: Experimental evidence and mechanistic insights, Geochimica et Cosmochimica Acta, 111, 39–49, doi:10.1016/j.gca.2012.09.004, 2013.

Knapp, D. R.: Handbook of Analytical Derivatization Reactions, John Wiley & Sons, New York, Chichester, Brisbane, Toronto, Singapore., 1979.

Konecky, B., Dee, S. G. and Noone, D. C.: WaxPSM: A Forward Model of Leaf Wax Hydrogen Isotope Ratios to Bridge Proxy and Model Estimates of Past Climate, Journal of Geophysical Research: Biogeosciences, 124, 2107–2125, doi:10.1029/2018JG004708, 2019.

Laursen, E. V., Thomsen, R. S. and Cappelen, J.: Observed Air Temperature, Humidity, Pressure, Cloud Cover and Weather in Denmark - with Climatological Standard Normals, 1961-90., 1999.

Levene, H.: Robust Tests for Equality of Variances, in Contributions to Probability and Statistics: Essays in Honor of Harold Hotelling, vol. 69, edited by I. Olkin, pp. 78–92, Standford University Press, Palo Alto, California., 1960.

Liu, W. and Yang, H.: Multiple controls for the variability of hydrogen isotopic compositions in higher plant *n*-alkanes from modern ecosystems, Global Change Biology, 14(9), 2166–2177, doi:10.1111/j.1365-2486.2008.01608.x, 2008.

Liu, Y., Wang, J., Liu, D., Li, Z., Zhang, G., Tao, Y., Xie, J., Pan, J. and Chen, F.: Straw mulching reduces the harmful effects of extreme hydrological and temperature conditions in citrus orchards, PLoS ONE, 9(1), 1–9, doi:10.1371/journal.pone.0087094, 2014.

McInerney, F. A., Helliker, B. R. and Freeman, K. H.: Hydrogen isotope ratios of leaf wax *n*-alkanes in grasses are insensitive to transpiration, Geochimica et Cosmochimica Acta, 75(2), 541–554, doi:10.1016/j.gca.2010.10.022, 2011.

Merlivat, L.: Molecular diffusivities of $H_2{}^{16}O$, $HD^{16}O$, and $H_2{}^{18}O$ in gases, The Journal of Chemical Physics, 69(6), 2864–2871, doi:http://dx.doi.org/10.1063/1.436884, 1978.

Mueller-Niggemann, C., Utami, S. R., Marxen, A., Mangelsdorf, K., Bauersachs, T. and Schwark, L.: Distribution of tetraether lipids in agricultural soils - Differentiation between paddy and upland management, Biogeosciences, 13(5), 1647–1666, doi:10.5194/bg-13-1647-2016, 2016.

Oppermann, B. I., Michaelis, W., Blumenberg, M., Frerichs, J., Schulz, H. M., Schippers, A., Beaubien, S. E. and Krüger, M.: Soil microbial community changes as a result of long-term exposure to a natural CO_2vent, Geochimica et Cosmochimica Acta, 74(9), 2697–2716, doi:10.1016/j.gca.2010.02.006, 2010.

Pedentchouk, N. and Zhou, Y.: Factors Controlling Carbon and Hydrogen Isotope Fractionation During Biosynthesis of Lipids by Phototrophic Organisms, in Hydrocarbons, Oils and

Lipids: Diversity, Origin, Chemistry and Fate. Handbook of Hydrocarbon and Lipid Microbiology, edited by H. Wilkes, pp. 1–24, Springer, Cham., 2018.

Peterse, F., van der Meer, J., Schouten, S., Weijers, J. W. H., Fierer, N., Jackson, R. B., Kim, J. H. and Sinninghe Damsté, J. S.: Revised calibration of the MBT-CBT paleotemperature proxy based on branched tetraether membrane lipids in surface soils, Geochimica et Cosmochimica Acta, 96, 215–229, doi:10.1016/j.gca.2012.08.011, 2012.

Prietzel, J., Dechamps, N. and Spielvogel, S.: Analysis of non-cellulosic polysaccharides helps to reveal the history of thick organic surface layers on calcareous Alpine soils, Plant and Soil, 365(1–2), 93–114, doi:10.1007/s11104-012-1340-2, 2013.

R Core Team: R: A Language and Environment for Statistical Computing, [online] Available from: https://www.r-project.org/, 2015.

Rach, O., Brauer, A., Wilkes, H. and Sachse, D.: Delayed hydrological response to Greenland cooling at the onset of the Younger Dryas in western Europe, Nature Geoscience, 7(1), 109–112, doi:10.1038/ngeo2053, 2014.

Rao, Z., Zhu, Z., Jia, G., Henderson, A. C. G., Xue, Q. and Wang, S.: Compound specific δD values of long chain *n*-alkanes derived from terrestrial higher plants are indicative of the δD of meteoric waters: Evidence from surface soils in eastern China, Organic Geochemistry, 40(8), 922–930, doi:http://dx.doi.org/10.1016/j.orggeochem.2009.04.011, 2009.

Romero-Viana, L., Kienel, U. and Sachse, D.: Lipid biomarker signatures in a hypersaline lake on Isabel Island (Eastern Pacific) as a proxy for past rainfall anomaly (1942-2006AD), Palaeogeography, Palaeoclimatology, Palaeoecology, 350–352, 49–61, doi:10.1016/j.palaeo.2012.06.011, 2012.

Sachse, D., Radke, J. and Gleixner, G.: Hydrogen isotope ratios of recent lacustrine sedimentary *n*-alkanes record modern climate variability, Geochimica et Cosmochimica Acta, 68(23), 4877–4889, doi:http://dx.doi.org/10.1016/j.gca.2004.06.004, 2004.

Sachse, D., Radke, J. and Gleixner, G.: δD values of individual *n*-alkanes from terrestrial plants along a climatic gradient – Implications for the sedimentary biomarker record, Organic Geochemistry, 37, 469–483, doi:10.1016/j.orggeochem.2005.12.003, 2006.

Sachse, D., Billault, I., Bowen, G. J., Chikaraishi, Y., Dawson, T. E., Feakins, S. J., Freeman, K. H., Magill, C. R., McInerney, F. A., van der Meer, M. T. J., Polissar, P., Robins, R. J., Sachs, J. P., Schmidt, H.-L., Sessions, A. L., White, J. W. C. and West, J. B.: Molecular Paleohydrology: Interpreting the Hydrogen-Isotopic Composition of Lipid Biomarkers from Photosynthesizing Organisms, Annual Reviews, 40, 221–249, doi:10.1146/annurev-earth-042711-105535, 2012.

Schäfer, I. K., Lanny, V., Franke, J., Eglinton, T. I., Zech, M., Vysloužilová, B. and Zech, R.: Leaf waxes in litter and topsoils along a European transect, SOIL, 2, 551–564, doi:10.5194/soil-2-551-2016, 2016.

Schlotter, D.: The spatio-temporal distribution of $\delta^{18}O$ and $\delta^{2}H$ of precipitation in Germany - an evaluation of regionalization methods, Albert-Ludwigs-Universität Freiburg im Breisgau. [online] Available from: http://www.hydrology.uni-freiburg.de/abschluss/Schlotter_D_2007_DA.pdf, 2007.

Schmidt, H.-L., Werner, R. A. and Roßmann, A.: ^{18}O Pattern and biosynthesis of natural plant products, Phytochemistry, 58(1), 9–32, doi:http://dx.doi.org/10.1016/S0031-

9422(01)00017-6, 2001.

Schmidt, H.-L., Werner, R. A. and Eisenreich, W.: Systematics of ^{2}H patterns in natural compounds and its importance for the elucidation of biosynthetic pathways, Phytochemistry Reviews, 2(1–2), 61–85, doi:10.1023/B:PHYT.0000004185.92648.ae, 2003.

Schouten, S., Hopmans, E. C. and Sinninghe Damsté, J. S.: The organic geochemistry of glycerol dialkyl glycerol tetraether lipids: A review, Organic Geochemistry, 54, 19–61, doi:10.1016/j.orggeochem.2012.09.006, 2013.

Schreuder, L. T., Beets, C. J., Prins, M. A., Hatté, C. and Peterse, F.: Late Pleistocene climate evolution in Southeastern Europe recorded by soil bacterial membrane lipids in Serbian loess, Palaeogeography, Palaeoclimatology, Palaeoecology, 449, 141–148, doi:10.1016/j.palaeo.2016.02.013, 2016.

Sessions, A. L., Burgoyne, T. W., Schimmelmann, A. and Hayes, J. M.: Fractionation of hydrogen isotopes in lipid biosynthesis, Organic Geochemistry, 30, 1193–1200, 1999.

Shapiro, S. S. and Wilk, M. B.: An Analysis of Variance Test for Normality, Biometrika, 52(3/4), 591–611, doi:/biomet/52.3-4.591, 1965.

Sternberg, L. S. L.: Comment on "Oxygen isotope ratios ($^{18}O/^{16}O$) of hemicellulose-derived sugar biomarkers in plants, soils and sediments as paleoclimate proxy I: Insight from a climate chamber experiment" by Zech et al. (2014), Geochimica et Cosmochimica Acta, 141, 677–679, doi:10.1016/j.gca.2014.04.051, 2014.

Strobl, C., Boulesteix, A. L., Zeileis, A. and Hothorn, T.: Bias in random forest variable importance measures: Illustrations, sources and a solution, BMC Bioinformatics, 8, doi:10.1186/1471-2105-8-25, 2007.

Strobl, C., Boulesteix, A. L., Kneib, T., Augustin, T. and Zeileis, A.: Conditional variable importance for random forests, BMC Bioinformatics, 9, 1–11, doi:10.1186/1471-2105-9-307, 2008.

Stumpp, C., Klaus, J. and Stichler, W.: Analysis of long-term stable isotopic composition in German precipitation, Journal of Hydrology, 517, 351–361, doi:10.1016/j.jhydrol.2014.05.034, 2014.

Sun, C. J., Zhang, C. L., Li, F. Y., Wang, H. Y. and Liu, W. G.: Distribution of branched glycerol dialkyl glycerol tetraethers in soils on the Northeastern Qinghai-Tibetan Plateau and possible production by nitrite-reducing bacteria, Science China Earth Sciences, 59(9), 1834–1846, doi:10.1007/s11430-015-0230-2, 2016.

Swedish Meteorological and Hydrological Institute: SMHI Open Data Meteorological Observations., 2018.

Tipple, B. J., Berke, M. A., Hambach, B., Roden, J. S. and Ehleringer, J. R.: Predicting leaf wax *n*-alkane $^{2}H/^{1}H$ ratios: Controlled water source and humidity experiments with hydroponically grown trees confirm predictions of Craig-Gordon model, Plant, Cell and Environment, 38(6), 1035–1047, doi:10.1111/pce.12457, 2015.

Tuthorn, M., Zech, M., Ruppenthal, M., Oelmann, Y., Kahmen, A., del Valle, H. F., Wilcke, W. and Glaser, B.: Oxygen isotope ratios ($^{18}O/^{16}O$) of hemicellulose-derived sugar biomarkers in plants, soils and sediments as paleoclimate proxy II: Insight from a climate transect study, Geochimica et Cosmochimica Acta, 126, 624–634,

903 doi:http://dx.doi.org/10.1016/j.gca.2013.11.002, 2014.

904 Tuthorn, M., Zech, R., Ruppenthal, M., Oelmann, Y., Kahmen, A., del Valle, H. F., Eglinton,
905 T., Rozanski, K. and Zech, M.: Coupling δ^2H and $\delta^{18}O$ biomarker results yields
906 information on relative humidity and isotopic composition of precipitation - a climate
907 transect validation study, Biogeosciences, 12, 3913–3924, doi:10.5194/bg-12-3913-
908 2015, 2015.

909 Umweltbundesamt GmbH: Erhebung der Wassergüte in Österreich gemäß Hydrographiegesetz
910 i.d.F. des BGBl. Nr. 252/90 (gültig bis Dezember 2006) bzw.
911 Gewässerzustandsüberwachung in Österreich gemäß Wasserrechtsgesetz, BGBl. I Nr.
912 123/06, i.d.g.F.; BMLFUW, Sektion IV / Abteilung 3 N. [online] Available from:
913 https://wasser.umweltbundesamt.at/h2odb/fivestep/abfrageQdPublic.xhtml (Accessed 20
914 September 2018), 2018.

915 Walker, C. D. and Brunel, J.-P.: Examining Evapotranspiration in a Semi-Arid Region using
916 Stable Isotopes of Hydrogen and Oxygen, Journal of Hydrology, 118, 55–75, 1990.

917 Wang, C., Hren, M. T., Hoke, G. D., Liu-Zeng, J. and Garzione, C. N.: Soil *n*-alkane δD and
918 glycerol dialkyl glycerol tetraether (GDGT) distributions along an altitudinal transect
919 from southwest China: Evaluating organic molecular proxies for paleoclimate and
920 paleoelevation, Organic Geochemistry, 107, 21–32,
921 doi:10.1016/j.orggeochem.2017.01.006, 2017.

922 Wang, H., Liu, W., Zhang, C. L., Liu, Z. and He, Y.: Branched and isoprenoid tetraether (BIT)
923 index traces water content along two marsh-soil transects surrounding Lake Qinghai:
924 Implications for paleo-humidity variation, Organic Geochemistry, 59, 75–81,
925 doi:10.1016/j.orggeochem.2013.03.011, 2013.

926 Weijers, J. W. H., Schouten, S., Spaargaren, O. C. and Sinninghe Damsté, J. S.: Occurrence
927 and distribution of tetraether membrane lipids in soils: Implications for the use of the
928 TEX_{86} proxy and the BIT index, Organic Geochemistry, 37(12), 1680–1693,
929 doi:10.1016/j.orggeochem.2006.07.018, 2006.

930 Weijers, J. W. H., Schouten, S., van den Donker, J. C., Hopmans, E. C. and Sinninghe Damsté,
931 J. S.: Environmental controls on bacterial tetraether membrane lipid distribution in soils,
932 Geochimica et Cosmochimica Acta, 71(3), 703–713, doi:10.1016/j.gca.2006.10.003,
933 2007.

934 Weijers, J. W. H., Wiesenberg, G. L. B., Bol, R., Hopmans, E. C. and Pancost, R. D.: Carbon
935 isotopic composition of branched tetraether membrane lipids in soils suggest a rapid
936 turnover and a heterotrophic life style of their source organism(s), Biogeosciences, 7(9),
937 2959–2973, doi:10.5194/bg-7-2959-2010, 2010.

938 Weijers, J. W. H., Steinmann, P., Hopmans, E. C., Schouten, S. and Sinninghe Damsté, J. S.:
939 Bacterial tetraether membrane lipids in peat and coal: Testing the MBT-CBT temperature
940 proxy for climate reconstruction, Organic Geochemistry, 42(5), 477–486,
941 doi:10.1016/j.orggeochem.2011.03.013, 2011.

942 Xie, S., Pancost, R. D., Chen, L., Evershed, R. P., Yang, H., Zhang, K., Huang, J. and Xu, Y.:
943 Microbial lipid records of highly alkaline deposits and enhanced aridity associated with
944 significant uplift of the Tibetan Plateau in the Late Miocene, Geology, 40(4), 291–294,
945 doi:10.1130/G32570.1, 2012.

946 Zech, M. and Glaser, B.: Compound-specific $\delta^{18}O$ analyses of neutral sugars in soils using gas

chromatography-pyrolysis-isotope ratio mass spectrometry: problems, possible solutions and a first application, Rapid Communications in Mass Spectrometry, 23, 3522–3532, doi:10.1002/rcm, 2009.

Zech, M., Rass, S., Buggle, B., Löscher, M. and Zöller, L.: Reconstruction of the late Quaternary paleoenvironments of the Nussloch loess paleosol sequence, Germany, using n-alkane biomarkers, Quaternary Research, 78(2), 226–235, doi:10.1016/j.yqres.2012.05.006, 2012a.

Zech, M., Kreutzer, S., Goslar, T., Meszner, S., Krause, T., Faust, D. and Fuchs, M.: Technical Note: *n*-Alkane lipid biomarkers in loess: post-sedimentary or syn-sedimentary?, Discussions, Biogeosciences, 9, 9875–9896, doi:10.5194/bgd-9-9875-2012, 2012b.

Zech, M., Tuthorn, M., Detsch, F., Rozanski, K., Zech, R., Zöller, L., Zech, W. and Glaser, B.: A 220 ka terrestrial $\delta^{18}O$ and deuterium excess biomarker record from an eolian permafrost paleosol sequence, NE-Siberia, Chemical Geology, doi:10.1016/j.chemgeo.2013.10.023, 2013.

Zech, M., Mayr, C., Tuthorn, M., Leiber-Sauheitl, K. and Glaser, B.: Reply to the comment of Sternberg on "Zech et al. (2014) Oxygen isotope ratios ($^{18}O/^{16}O$) of hemicellulose-derived sugar biomarkers in plants, soils and sediments as paleoclimate proxy I: Insight from a climate chamber experiment. GCA, Geochimica et Cosmochimica Acta, 141(0), 680–682, doi:10.1016/j.gca.2014.04.051, 2014.

Zech, M., Zech, R., Rozanski, K., Gleixner, G. and Zech, W.: Do *n*-alkane biomarkers in soils/sediments reflect the $\delta^{2}H$ isotopic composition of precipitation? A case study from Mt . Kilimanjaro and implications for paleoaltimetry and paleoclimate research, Isotopes in Environmental and Health Studies, 51(4), 508–524, doi:10.1080/10256016.2015.1058790, 2015.

Zech, R., Gao, L., Tarozo, R. and Huang, Y.: Branched glycerol dialkyl glycerol tetraethers in Pleistocene loess-paleosol sequences: Three case studies, Organic Geochemistry, 53, 38–44, doi:10.1016/j.orggeochem.2012.09.005, 2012c.